Summer 2024

A Kinematic Analysis of the Shoulder During the Volleyball Attack Using Euler and Helical Axis Methods

Victoria Jolliff
Old Dominion University, victoriarjolliff@gmail.com

A KINEMATIC ANALYSIS OF THE SHOULDER DURING THE VOLLEYBALL ATTACK USING EULER AND HELICAL AXIS METHODS

by

Victoria Jolliff
B.S. May 2022, West Virginia University

A Thesis Submitted to the Faculty of
Old Dominion University in Partial Fulfillment of the
Requirements for the Degree of

MASTER OF SCIENCE

BIOMEDICAL ENGINEERING

OLD DOMINION UNIVERSITY
August 2024

Approved by:

Stacie I. Ringleb (Director)

Hunter J. Bennett (Member)

Sebastian Y. Bawab (Member)

ABSTRACT

A KINEMATIC ANALYSIS OF THE SHOULDER DURING THE VOLLEYBALL ATTACK USING EULER AND HELICAL AXIS METHODS

Victoria Jolliff
Old Dominion University, 2024
Director: Dr. Stacie I. Ringleb

The shoulder is a complex joint with a wide range of motion, including flexion, extension, abduction, adduction, and internal and external rotation. In volleyball, repetitive overhand movements can cause shoulder overuse injuries. The primary offensive move, the attack, involves the approach, arm cocking, arm acceleration, and follow-through phases. Motion capture analysis and techniques like calculating Euler angles and rotation about a mean helical axis can evaluate shoulder movements. This study aimed to calculate shoulder movements during each phase of the volleyball attack using the Euler angle YXY sequence and the helical axis method. Different attack types, such as cross-court and line attacks, as well as cross-body and same-side follow-through strategies, were compared. Sixteen highly competitive or professional volleyball players participated, completing a series of attacks with varying directions and follow-through strategies in random order. Data were processed in Visual3d, and kinematics were calculated using custom MATLAB programs. Results indicated that the helical axis method revealed patterns of shoulder movements during the approach phase, suggesting that arm cocking might begin before takeoff. Both methods showed minimal variation during the arm cocking phase. Significant differences in the angle of elevation were observed during the arm acceleration phase between cross-court cross-body and line same-side attacks. The follow-through phase showed differences, with cross-body attacks involving more dynamic shoulder

movements and same-side attacks exhibiting smoother motions. These findings highlight distinct shoulder mechanics in different volleyball strategies and underscore the helical axis method's effectiveness in optimizing performance and preventing injuries.

I dedicate this thesis to my dad, who has always been my biggest role model and whose encouragement has been instrumental in making this achievement possible. Your belief in my potential and your constant encouragement have been a driving force throughout my journey. Thank you for inspiring me to pursue my dreams and for always being there to support me along the way. To my mom, for always having my back with unwavering support. Your endless sacrifices have allowed me to pursue my goals in all facets of life. Whether it was cheering me on during my achievements or comforting me during tough times, you have always been my greatest supporter. I am deeply grateful for everything you have done for me. To my brother, Justin, for providing me with a loving home throughout my studies. Your support has been invaluable on this journey. To the rest of my family and friends back home who supported me as I moved across state lines to pursue my educational goals, thank you for understanding as I navigated this chapter of my life. To my high school math teachers, Ms. Swails, Mr. Freeland, Mrs. Farley, and Mr. Snider, who may never read this, but whose guidance and inspiration were deeply pivotal in my life. To my lab mates, Nathan, Isaac, and Abed (aka, "The Ringlabers"), whose friendship has been an integral part of my journey. From our road trip to Knoxville, our daily de-stress walks, and our unique ability to find all the free food on campus, the memories we have made will stay with me wherever I go. I'll truly miss our time together. To my fiancé, Garrett, for being my calm in the storm. From the late nights to the moments of doubt and stress, you were always there to offer a comforting word and a reassuring presence. Your belief in me, even when I doubted myself, has been a constant source of strength. You've celebrated my victories and helped me through the challenges with grace and patience. I hope to be that support system for you as you follow your dreams. Lastly, to my younger self, for dreaming big and never giving up. I think you would be proud of where we are today.

ACKNOWLEDGMENTS

I would like to thank my committee members, Dr. Stacie Ringleb, Dr. Hunter Bennett, and Dr. Sebastian Bawab, for their guidance and support throughout this research. I am particularly grateful to Dr. Ringleb for her exceptional mentorship and for providing me with the opportunity to study biomechanics. Her expertise, feedback, and encouragement have been integral to the success of this project. Additionally, I extend my thanks to Dr. Kiara Barrett for her efforts in collecting the volleyball data and for graciously allowing me to analyze it as part of this study. Without her hard work, this would not be possible. Lastly, I would like to thank my lab mates, Dr. Nathan Holland, Isaac Kumi, and Abed Khosrojerdi, for their help and guidance. Their camaraderie made the lab a safe and welcoming space to work, and I owe much of this progress to their collaboration and insights.

TABLE OF CONTENTS

Page

LIST OF FIGURES

LIST OF TABLES

Table Page

CHAPTER 1

INTRODUCTION

The shoulder joint, also known as the glenohumeral joint, is a ball-and-socket joint formed by the articulation between the head of the humerus and the glenoid cavity of the scapula (Figure 1). This joint has the largest range of motion of any joint in the body. However, this freedom of movement is due to minimal structural support, and thus, the enhanced mobility is offset by a loss of stability (Biga et al., 2019). Understanding the kinematics of the shoulder is not just a matter of academic interest, but a need for improving performance and preventing injuries in both daily activities and sports maneuvers.

Figure 1. Anatomy of the shoulder

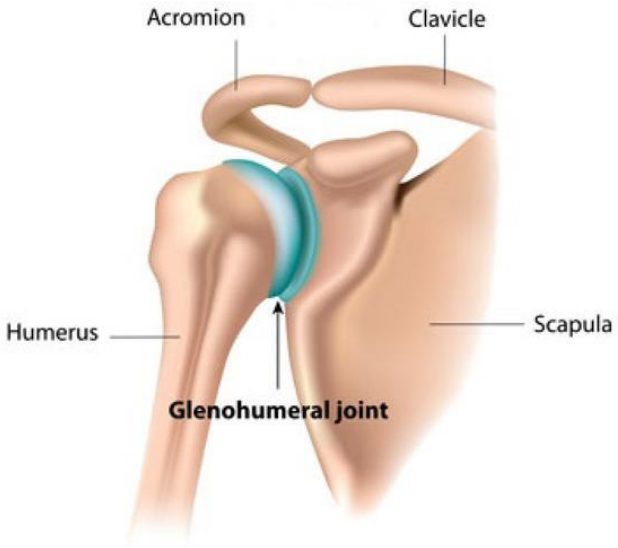

Note: Reproduced from Delgado et al., 2001, used under Creative Commons CC-BY license.

Volleyball unites people of all ages and backgrounds through its dynamic and engaging gameplay. The governing body of volleyball estimates that there are 800 million players globally

across more than 200 countries, making it one of the most widely played sports in the world (Fédération Internationale de Volleyball, n.d.). Given its popularity, it is important to understand how biomechanics can influence player performance, prevent injury, and enhance training practices.

1.1 Shoulder Kinematics

The shoulder joint, comprising the scapula, clavicle, humerus, and thorax, exhibits remarkable mobility to facilitate the large range of motion (ROM) necessary for performing the volleyball attack. It allows for arm movements such as abduction and adduction, which brings the upper limb away (ab) and towards (ad) the body's midline. Also, the shoulder can perform flexion (raising the arm anterior in the sagittal plane) and extension (extending the arm posterior in the sagittal plane) (Figure 2). Lastly, internal rotation and external rotation occur when the arm rotates inward and outward along a vertical axis. The International Society of Biomechanics (ISB) defines the shoulder joint's anteroposterior axis as X_h, the longitudinal axis as Y_h, and the mediolateral axis as Z_h, (Figure 3) (Wu et al., 2005). This indicates that ab/ad-duction is in the X direction, internal/external rotation is in the Y direction, and flexion/extension is in the Z direction.

Figure 2. Shoulder planar movements

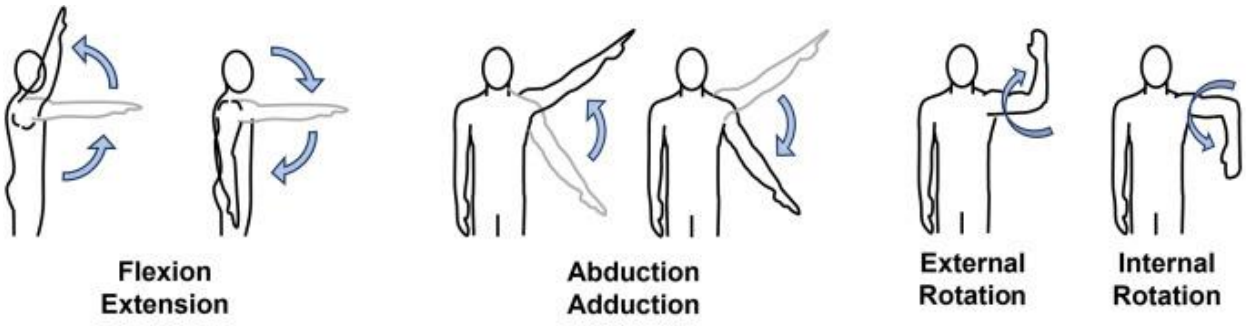

Note: Adapted from Kritzer et al., 2024, used under Creative Commons CC-BY license.

Figure 3. Shoulder coordinate system

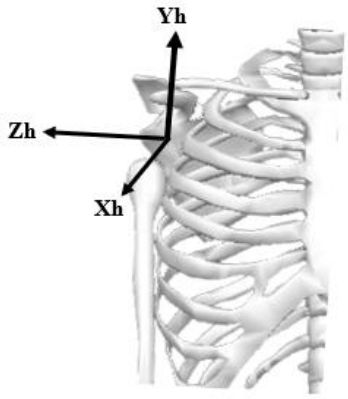

The shoulder has an extensive range of motion (ROM), with total abduction and flexion being the largest, reaching up to 185 degrees each (Table 1) (Bakhsh & Nicandri, 2018). Various factors, including age, activity level, and any existing medical conditions, can influence ROM. Clinically, total ROM is usually measured using a goniometer, which helps physicians determine the angle between the humerus and the torso across six specific movements. ROM for a particular activity is more difficult to measure, especially in a dynamic movement, because movement usually occurs in all three planes of motion. ROM and other factors such as muscle activation, coordination, and strength all influence the kinematics of the shoulder.

Table 1. Reported ROM values for each shoulder movement.

Movement	Total ROM (º)
Flexion	185
Extension	65
Abduction	185
Adduction	55
Internal Rotation	75
External Rotation	95

1.2 The Volleyball Attack

A central component of offensive strategy in volleyball is the attack, designed to score points by a combination of ball speed and strategic placement (Challoumas & Artemious, 2018). The volleyball attack is a complex, multiphase action comprising the approach, take-off, arm cocking, arm swing, and follow-through (Figure 4) (Reeser et al., 2010; Zahálka et al., 2017).

Figure 4. The volleyball attack phases.

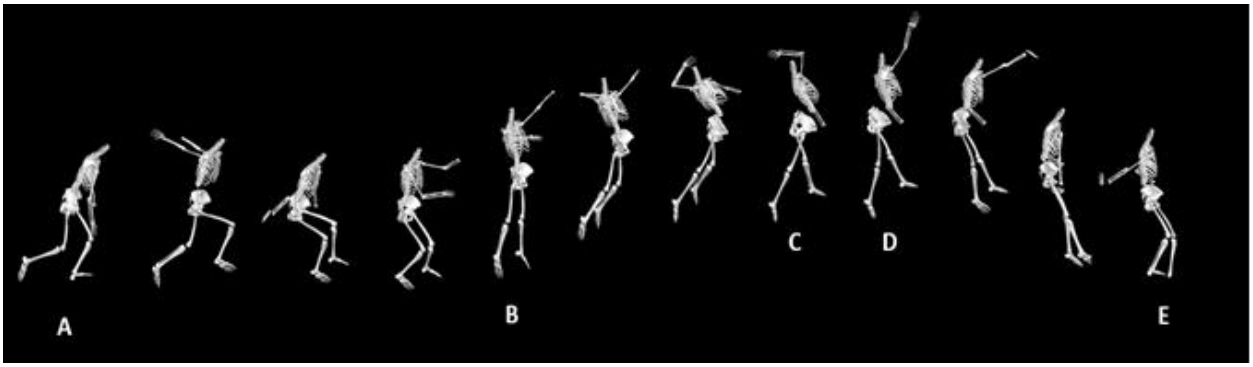

Note: The approach (A → B), arm cocking (B → C), arm acceleration (C → D), and follow-through (D → E). The takeoff (B), maximum external rotation (C), and hand contact (D) separate the phases.

Players choose either a 3 or 4-step approach leading into the takeoff posture. This leads to the takeoff jump and arm cocking, where the player prepares to strike the volleyball by abducting and externally rotating the shoulder. The player then quickly accelerates the arm by flexing and internally rotating the upper arm, making ball contact. Depending on the strategy of the play, the player will choose a direction to spike the ball towards. These directions, or targets, are commonly either cross-court, where the goal is to hit the ball at an angle towards the opposite side of the court, or line, where the goal is to hit the ball straight again. The maximum external rotation of the shoulder is used to separate arm cocking and arm acceleration. Players choose to

follow-through with their arm either on the same side or across the body (Reeser et al., 2010). This coordinated sequence of movements aims to deliver powerful and precise hits, challenging the opposing team's ability to defend and securing points.

Each play begins with a serve to the opposing team, followed by a continuous cycle of passing, setting, and attacking until the ball touches the floor, signaling the end of the play. This repetitive nature requires players to perform attacks frequently. An elite volleyball player training 16-20 hours a week will perform about 40,000 attacks annually (Kugler et al., 1996). Because of this, shoulder injuries are common. At the instant of ball contact, shoulder abduction reaches approximately 130 degrees, much greater than similar movements in other sports, such as the tennis serve and baseball pitch (Reeser et al., 2010). This potentially leads to an elevated risk of subacromial impingement or labral damage (Chu et al., 2009; Elliot et al., 2003; Reeser et al., 2010). Consequently, shoulder injuries are the fourth-most reported injury among NCAA women's volleyball players, with 50.9% classified as inflammatory or impingement (Chandran et al., 2021).

1.3 Motion Capture and Kinematic Analysis

Obtaining and analyzing shoulder motion is challenging, given the complexity of the shoulder. Many biomechanists turn to motion capture technology for these tasks. The Vicon (Vicon Motion Systems Ltd, Oxford, UK) system captures body movement using an array of infrared cameras situated around the subject. The cameras detect and track the movement of reflective markers strategically placed on the skin of the subject. The marker data collected through motion capture can be used to build a model and perform analyses of the shoulder's motion. This data can be used to create a kinematic analysis of the shoulder joint, which generates a series of rotation matrices for a particular movement (Goldfarb et al., 2021).

Despite motion capture advancements, standardizing the method for calculating shoulder joint angles remains a challenge. This is because, in most sports-related tasks, ROM in all three planes is nearly exhausted, while other movements usually involve movement in one primary plane, with the other two serving supportive roles. Consequently, the literature does not agree on a standard method of calculating shoulder joint angles. Two methods have been proposed for representing the orientation between two body segments in three-dimensional space: Euler angles and helical axes (Chao, 1980; Woltring, 1991). The most common method for the estimation of 3D joint motion is to use Euler or Cardan angles (Wu et al., 2005). However, conflicting findings state that measuring the helical axis of the complex movement more accurately describes the motion (Phadke et al., 2011). Each method has its own advantages and disadvantages, which contribute to discrepancies in accuracy and interpretability.

1.3.1 Euler Angle Method

Euler angles are a set of three sequence-dependent rotations about three axes. To create a standard to define joint motion in 3D space, the ISB recommends calculating the Euler angles using specific rotation sequences for each joint, using the YXY sequence for the shoulder (Wu et al., 2005).

One of the advantages of using Euler angles to describe shoulder angles is their intuitive understanding. They correspond to rotations about anatomical axes, making them easy to visualize and interpret. They align well with the natural movements of the shoulder, such as flexion/extension, abduction/adduction, and internal/external rotation. Additionally, they are mathematically straightforward to derive from rotation matrices, which can easily be extracted from the marker data.

However, there are significant limitations to using Euler angles for shoulder joint analysis. A major drawback is a phenomenon known as gimbal lock, which occurs when two of

the three rotation axes align, causing a loss of one degree of freedom and making certain orientations undefined or ambiguous. This can be problematic when analyzing complex shoulder movements that involve large ranges of motion. Moreover, the angles are dependent on the chosen rotation sequence, which can affect the interpretation and inter-study comparisons. Additionally, Euler angles with the first and third rotation about the same axis, e.g., the YXY sequence, can lead to confusion in anatomical interpretation.

1.3.2 Helical Axis Method

The helical axis method, also known as the screw axis, is a technique used to describe the orientation and movement of the shoulder joint in three-dimensional space. This method has been suggested to study joint kinematics but has not been formally adopted as the standard (Cattrysse et al. 2007; Cripton et al. 2001; Helena Grip et al. 2008; Woltring et al. 1985). This method involves defining a helical axis about which a body segment rotates and translates. The helical axis is characterized by a unit vector indicating its orientation and an associated angle of rotation. The X, Y, and Z components of the unit vector describe the helical axis with respect to the shoulder axis system. It is particularly useful in biomechanics for capturing the complex and multi-planar motions of the shoulder, such as those performed during a volleyball attack.

One of the primary advantages of the helical axis method is its ability to represent both rotational and translational components of movement in a comprehensive parameter. This method captures the true nature of the shoulder's motion, as the shoulder joint often involves coupled rotations and translations due to its ball-and-socket structure. Additionally, the helical axis method does not suffer from the same limitations as Euler angles, such as gimbal lock. This could be an improvement for analyzing large ranges of motion without losing information about the orientation of the joint. However, the helical axis method also has its limitations. The helical axis does not provide a representation of joint orientation in terms of three anatomically and

clinically meaningful parameters. This could lead to confusion of interpretation between researchers and physicians.

1.4 Study Purpose

This study reviews the biomechanics of the shoulder during a volleyball attack, with a particular focus on calculating shoulder joint angles and analyzing kinematics. The research has three primary objectives. First, it aims to calculate and compare the shoulder joint kinematics during a volleyball attack using both Euler angles and helical axis methods. The study breaks down the complex movement of the volleyball attack into phases: approach, arm cocking, arm acceleration, and follow-through. Calculating the kinematics using Euler angles and helical axis could reveal patterns in the shoulder motion within each phase.

Second, the study analyzes the statistical differences in shoulder kinematics based on the direction (cross-court vs. line) and follow-through (cross-body vs. same-side) of the attack. This analysis aims to offer insights into how different attacking strategies affect shoulder biomechanics and to inform coaching techniques that could optimize performance and minimize injury risks.

Finally, the study compares the interpretability of the Euler angles and helical axis methods in representing shoulder kinematics. It explores whether the Helical Axis method can reveal aspects of shoulder kinematics that are not apparent with Euler angles, thereby assessing the potential advantages of HA in biomechanical analysis. The main motivation in comparing both methods is if the Helical axis method can provide additional information that are not consistent or well understood in the Euler angle method. This study aims to investigate best practices for future biomechanical analyses and deepen the understanding of shoulder joint mechanics during the volleyball attack.

CHAPTER 2

METHODS

2.1 Participants

22 volunteers from members of the Tidewater Volleyball Association and the Association of Volleyball Professionals participated in this study. Due to data processing challenges, 16 of the 22 participants were included in the analysis (Table 2). The inclusion criteria for player participation required ages between 18 and 35 years and competition at the AA level or higher. The AA level is described as containing highly competitive players, college athletes, or professionals (*Leagues*, n.d.). Participants were excluded if they were experiencing shoulder pain, had any injuries, or received significant orthopedic surgery in the previous six months.

Table 2. Participant characteristics

	Age (yrs)	Height (m)	Weight (kg)	Experience (yrs)
Male	26 (4)	1.85 (0.08)	84.47 (12.83)	10.31 (3.40)
Female	25 (5)	1.77 (0.08)	70.88 (10.02)	11.36 (5.24)

2.2 Testing Protocol

Participants provided informed consent and completed a medical history questionnaire to ensure eligibility for the study. Data collection proceeded only if all inclusion criteria were met. Data were collected using a Vicon 12-camera 3D motion capture system in a laboratory setting, which recorded trunk and upper extremity motion at a 250 Hz sampling rate. Anatomical markers were placed on the right and left acromion, medial and lateral humeral epicondyles, and medial and lateral wrists. Tracking markers were placed on the posterior side of each shoulder,

the inferior angle of the dominant arm scapula, C7 bone, sternum, index and ring fingers, and dorsal side of the hand. Tracking clusters were placed on the upper and lower arms (Figure 5).

Figure 5. Marker set placement.

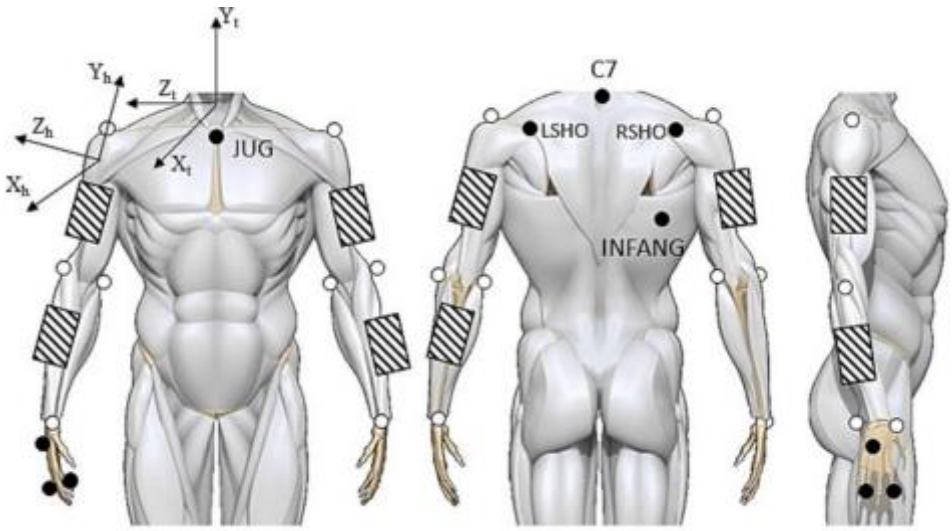

Each participant was required to perform a total of 20 attacks after completing a self-guided warm-up. To analyze the directional differences, participants completed 5 trials for each of the 4 trial conditions. Participants were instructed to perform their normal approach and takeoff. The four trial conditions consisted of 2 target directions and 2 follow-through strategies. The 2 targets included cross-court and line shots, where participants were instructed to simulate these attacks as closely as possible. The 2 follow-throughs were categorized as either cross-body or same-side. Participants were instructed to end their attack with their dominant arm on the contralateral hip for the cross-body follow-through and ipsilateral hip for the same-side. To remain concise, conditions will herein be referred to as Cross_CB (cross-court attack with cross-body follow-through), Cross_SS (cross-court attack with same-side follow-through), Line_CB (line attack with cross-body follow-through), and Line_SS (line attack with same-side follow-through).

Combinations of the attack direction and follow-through resulted in 4 trial conditions (Table 3). Each was assigned in a random order to each participant, ensuring that all conditions were evenly represented, and potential order effects were minimized. Due to data processing difficulties, the most successful trial for each condition was used for analysis.

Table 3. Trial Conditions

Condition Name	Description
Cross_CB	Cross-court attack and cross-body follow-through
Cross_SS	Cross-court attack and same-side follow-through
Line_CB	Line attack and cross-body follow-through
Line_SS	Line attack and same-side follow-through

2.3 Data Processing

Data were processed using Visual3d (version 6; C-Motion, Inc.). A kinematic model was created according to the method detailed by Barrett et al. (2024). Briefly, an upper arm cluster was used to track the humerus, while markers on the left and right shoulders, C7, inferior angle, and jugular notch were used to track the trunk in a kinematic model. In accordance with ISB guidelines, segmental coordinate systems were defined for the hand, forearm, and humerus (Wu et al., 2005). The ISB-recommended T8 marker was replaced with a marker on the inferior angle of the dominant limb, as recommended by Haneline et al. (2008), due to participant attire. The offset of the separation between the left and right acromion markers was used to calculate the shoulder joint center (Rab et al., 2002).

Data were filtered using a 4th-order zero-lag Butterworth filter with a cutoff frequency of 30Hz. The takeoff, maximum external rotation, and hand contact were labeled to separate each phase of the attack. Shoulder rotation matrices were extracted from rotations of the dominant arm humerus relative to the thorax. Because Visual 3D uses passive (alias) rotation and

MATLAB uses active (alibi) rotation, the rotation matrices from Visual3d were transposed prior to additional analysis to match between software.

The kinematics of the approach phase, arm cocking phase, arm acceleration phase, and follow-through phase were individually analyzed to identify differences in phase patterns. Each phase was defined based on specific points in the attack motion. The attack began when the participant initiated the first step in the approach. Takeoff was marked as the moment the feet left the ground, distinguishing the approach phase from the arm cocking phase. The transition between the arm cocking and arm acceleration phases was identified at the maximum external rotation of the shoulder, seen as the most negative point on a graph of shoulder axial rotation. Hand contact, which separates the arm acceleration and follow-through phases, was noted at the instant the hand contacted the ball. The end of the attack was defined as the point where the arm reached the final position of the respective follow-through motion. For the cross-body follow-through, this is when the hand is most aligned with the contralateral hip, or when maximum adduction occurs by visual inspection. The same-side follow-through is when the shoulder reaches maximum extension on the ipsilateral side.

2.3.1 Euler Angle Calculation

The YXY Eulerian sequence was applied to all data, representing the current standard. Euler angles were calculated from rotation matrices extracted from Visual3d using a custom MATLAB program (appendices). The calculation is derived using the formula outlined in Eberly (1999). Due to differences in the shoulder axis system and the conventional axis system where Z is the longitudinal axis, the ZXZ sequence formula was used. However, this is equivalent to the shoulder YXY sequence.

The MATLAB program used to calculate the Euler angles was created from the following rotation matrix derivation. The YXY Euler angles were calculated as the plane of elevation (θy_0), angle of elevation (θx), and the internal/external rotation (θy_1). The rotation about the x-axis (1) and y-axis (2) by angle θ is multiplied in sequence order and equated (3).

$$Rx = \begin{bmatrix} 1 & 0 & 0 \\ 0 & cos\theta & -sin\theta \\ 0 & sin\theta & cos\theta \end{bmatrix} \quad (1)$$

$$Ry = \begin{bmatrix} cos\theta & 0 & sin\theta \\ 0 & 1 & 0 \\ -sin\theta & 0 & cos\theta \end{bmatrix} \quad (2)$$

$$Ry(\theta y_0)Rx(\theta x)Ry(\theta y_1) = \begin{bmatrix} r_{11} & r_{12} & r_{13} \\ r_{21} & r_{22} & r_{23} \\ r_{31} & r_{32} & r_{33} \end{bmatrix} = \begin{bmatrix} c_{y_0}c_{y_1} - c_x s_{y_0} s_{y_1} & -c_x c_{y_1} s_{y_0} - c_{y_0} c_{y_1} & s_x s_{y_0} \\ c_{y_1} s_{y_0} + c_x c_{y_0} s_{y_1} & c_x c_{y_0} c_{y_1} - s_{y_0} s_{y_1} & -s_x c_{y_0} \\ s_x s_{y_1} & s_x c_{y_1} & c_x \end{bmatrix} \quad (3)$$

The rotation matrix generated from Visual3d is equated to (3) and the values are used to calculate the plane of elevation (4), angle of elevation (5), and internal/external rotation (6).

$$\theta y_0 = \text{atan2}(r13, -r23) \quad (4)$$

$$\theta x = \text{acos}(r33) \quad (5)$$

$$\theta y_1 = \text{atan2}(r31, r32) \quad (6)$$

When r33 = 1, $\theta x = 0$. Thus, the equations for plane of elevation (5), angle of elevation (6), and internal/external rotation (7) can be used to calculate the angles for this case.

$$\theta y_0 = \text{atan2}(-r12, r11) \quad (7)$$

$$\theta x = 0 \quad (8)$$

$$\theta y_1 = 0 \quad (9)$$

When r33 = -1, θx = π. The equations for plane of elevation (8), angle of elevation (9), and internal/external rotation (10) can be used to calculate the angles for this case.

$$\theta y_0 = -\text{atan2}(-r12, r11) \quad (8)$$

$$\theta x = \pi \quad (9)$$

$$\theta y_1 = 0 \quad (10)$$

To validate the calculation of the Euler angles, a side-by-side comparison of the calculated Euler angles and those extracted from Visual 3D for a representative subject is compared (Figure 6). Once the Euler angle calculation was validated, the angles were then normalized to 100 points and averaged across phases and conditions to determine the plane of elevation, angle of elevation, and internal/external mean angles. Additionally, the maximum, minimum, and ROM for each movement was determined for kinematic analysis.

Figure 6. Euler Angles (°) Comparison from a Representative Subject

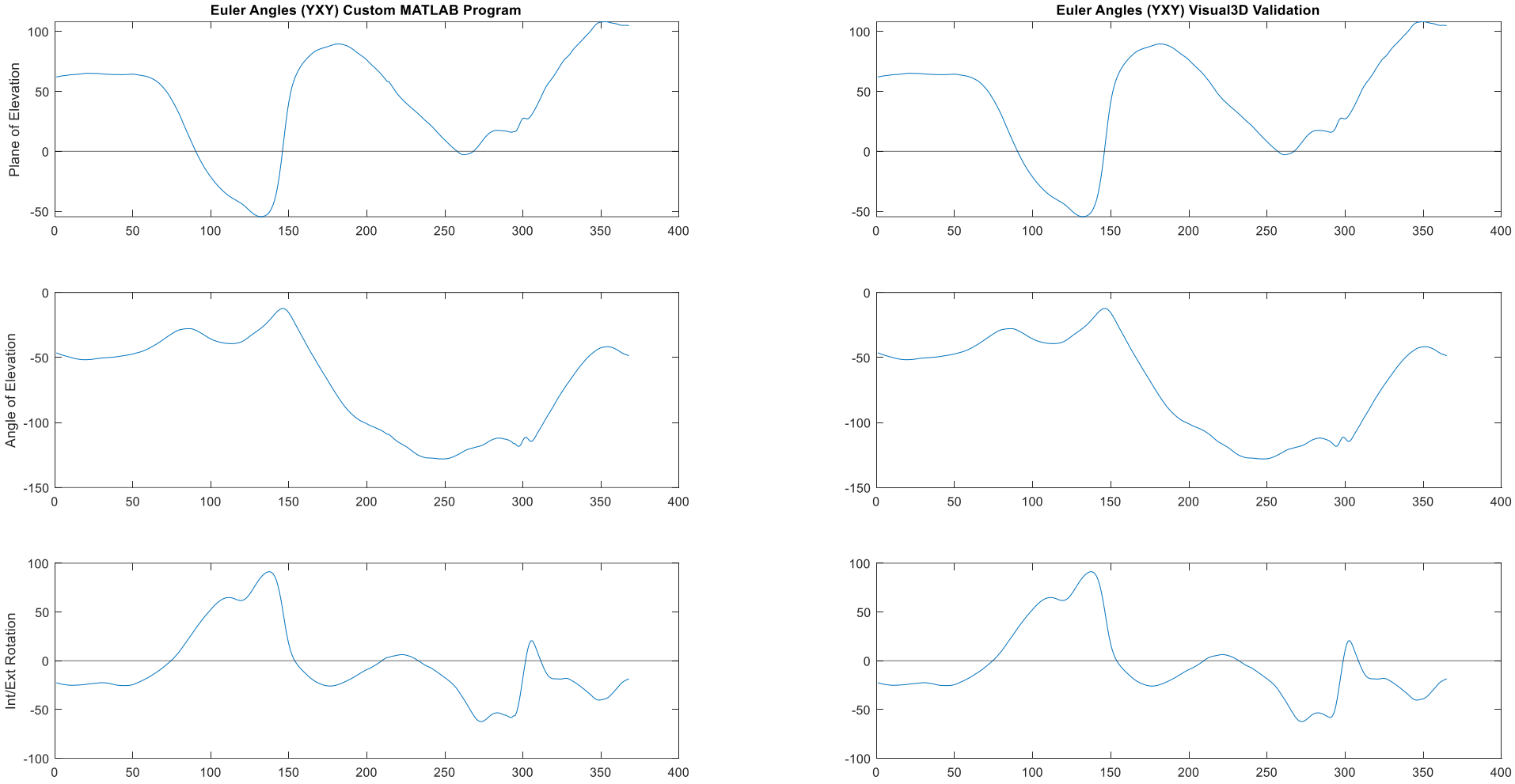

2.3.2 FHA Calculation

The finite helical axis (FHA) for each frame was calculated using the method proposed by Spoor and Veldpaus (1980) in a custom MATLAB program. The program accepts the input of the shoulder rotation matrices and outputs the unit vector of an angle of rotation about the helical axis. The angle of rotation can be calculated using the rotation matrix, where $R_{x,y}$ indicate the elements of the specific rotation matrix for each frame (11,12,13). The unit vector's X, Y, and Z components were calculated using equation (14). The angle of rotation and unit vector were determined for each phase and condition, normalized to 100 points, and plotted to visualize the kinematics over the length of each phase.

$$\sin(\varphi) = \frac{1}{2}\sqrt{(R_{3,2} - R_{2,3})^2 + (R_{1,3} - R_{3,1})^2 + (R_{2,1} - R_{1,2})^2} \tag{11}$$

$$\cos(\varphi) = \frac{1}{2}(R_{1,1} + R_{2,2} + R_{3,3} - 1) \tag{12}$$

$$\varphi = \begin{cases} \arcsin(\sin(\varphi)) \mid \sin(\varphi) \leq \frac{\sqrt{2}}{2} \\ \arccos(\cos(\varphi)) \mid \sin(\varphi) > \frac{\sqrt{2}}{2} \end{cases} \tag{13}$$

$${}^{1}\boldsymbol{n}_{FHA} = \frac{1}{2\sin(\varphi)} \begin{bmatrix} R_{3,2} - R_{2,3} \\ R_{1,3} - R_{3,1} \\ R_{2,1} - R_{1,2} \end{bmatrix}^T \tag{14}$$

To determine if there was major subject variability in the helical axis orientation and angle of rotation, two representative participants were compared for differences between these angles (Figure 7). This was performed to determine if additional analyses of individual differences would help better predict kinematics associated with the full attack.

Figure 7. Helical Axis Orientation and Angle of Rotation from Two Representative Subjects

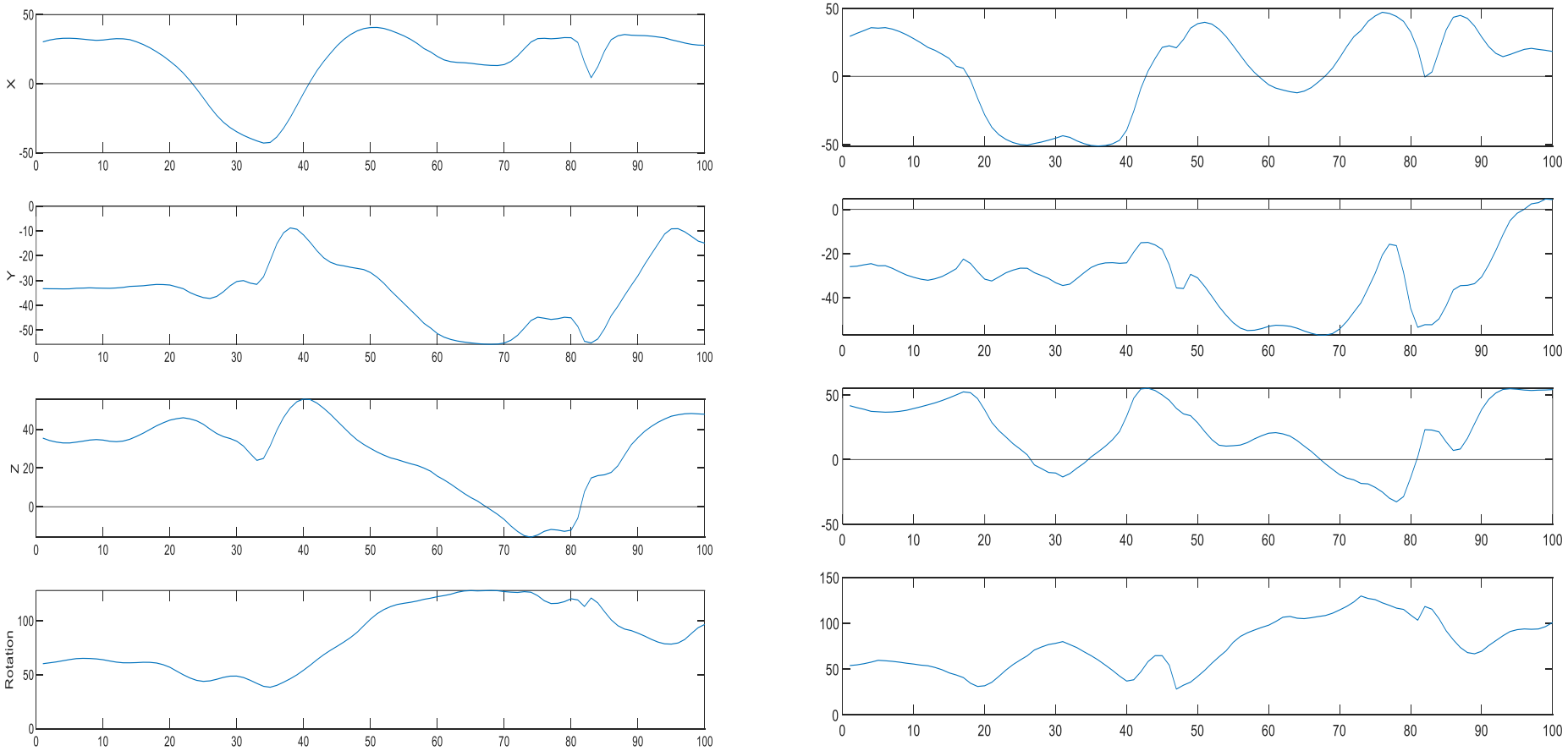

2.3.3 Statistical Analyses

To analyze differences in the Euler angles and the angle of rotation about the HA across direction and follow-through conditions, one-way repeated measures ANOVA ($p<0.05$) testing was performed. Normality was either confirmed or violated using the Shapiro-Wilk test. If data violated normality ($p<.05$), nonparametric repeated measures ANOVA testing was performed. All conditions were compared for significance across each phase. All statistical analyses were performed in SPSS (Version 29.0.1.0)

CHAPTER 3

RESULTS

3.1 Full Attack

The helical axis direction vector and angle of rotation for the full attack were calculated and plotted. In the cross-court cross-body attack (Figure 8), the helical axis direction vector shows a consistent orientation during the approach phase, with significant reorientation occurring at the arm cocking phase, indicating preparation for the arm swing. The angle of rotation increases sharply during the arm acceleration phase, reflecting the rapid shoulder movement required for ball contact. These results are similar across each attack type (Figure 9, 10, & 11).

Figure 8. HA Direction Vector and Rotation (°) Cross-Court, Cross-Body Attack

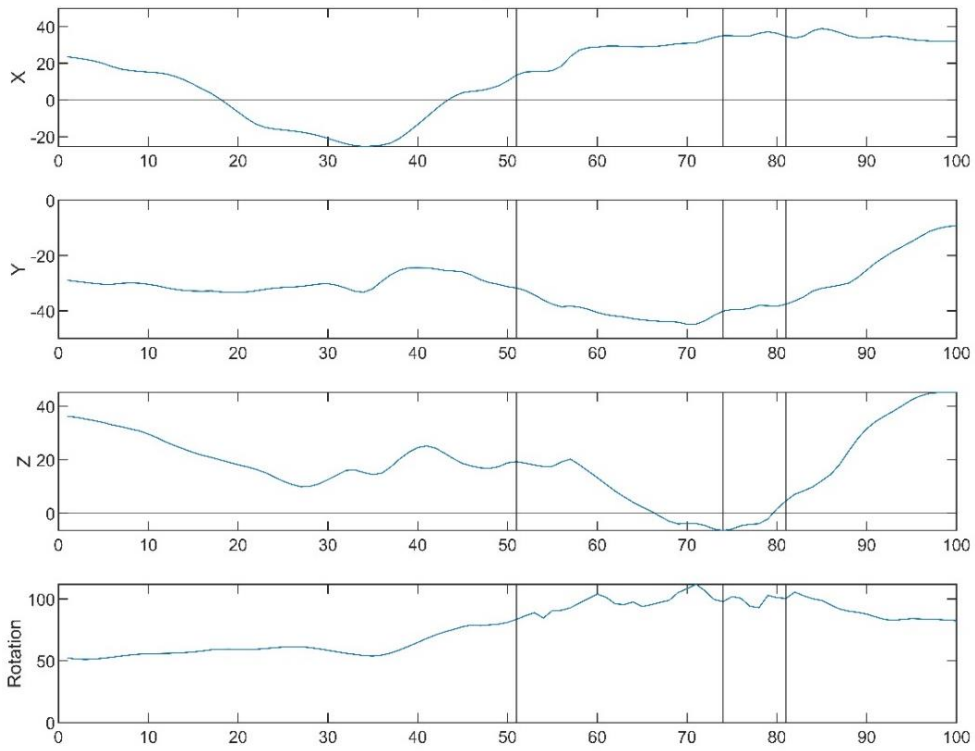

Note: First line indicates the takeoff, second line indicates maximum external rotation of the shoulder, and third line indicates hand contact with the ball for all subsequent plots.

Figure 9. HA Direction Vector and Rotation (°) Cross-Court, Same-Side Attack

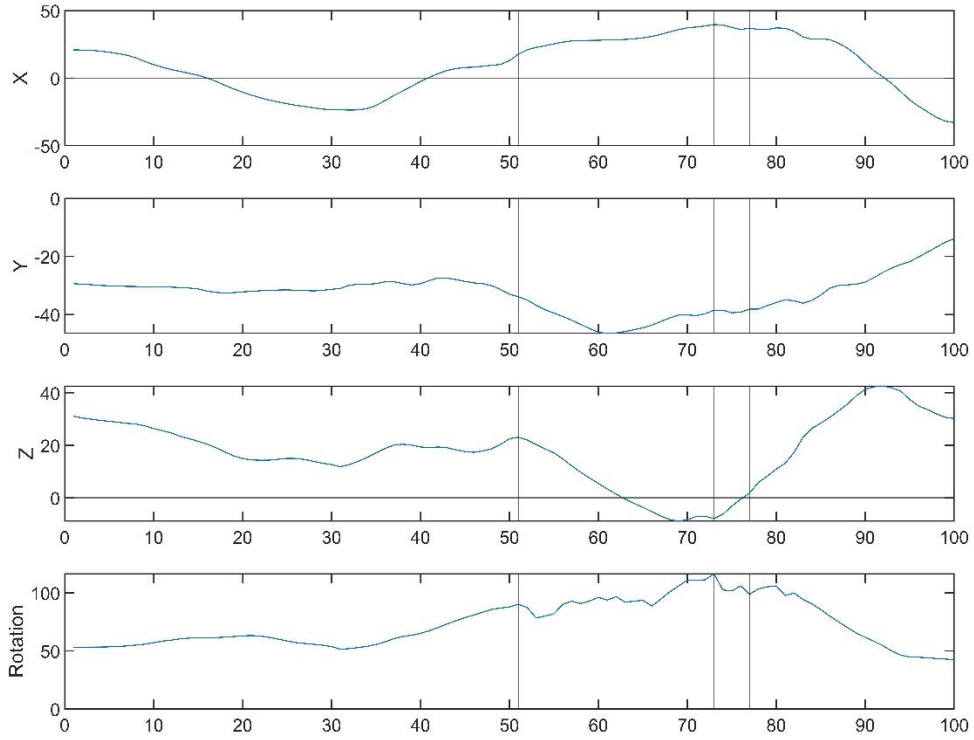

Figure 10. HA Direction Vector and Rotation (°) Line, Cross-Body Attack

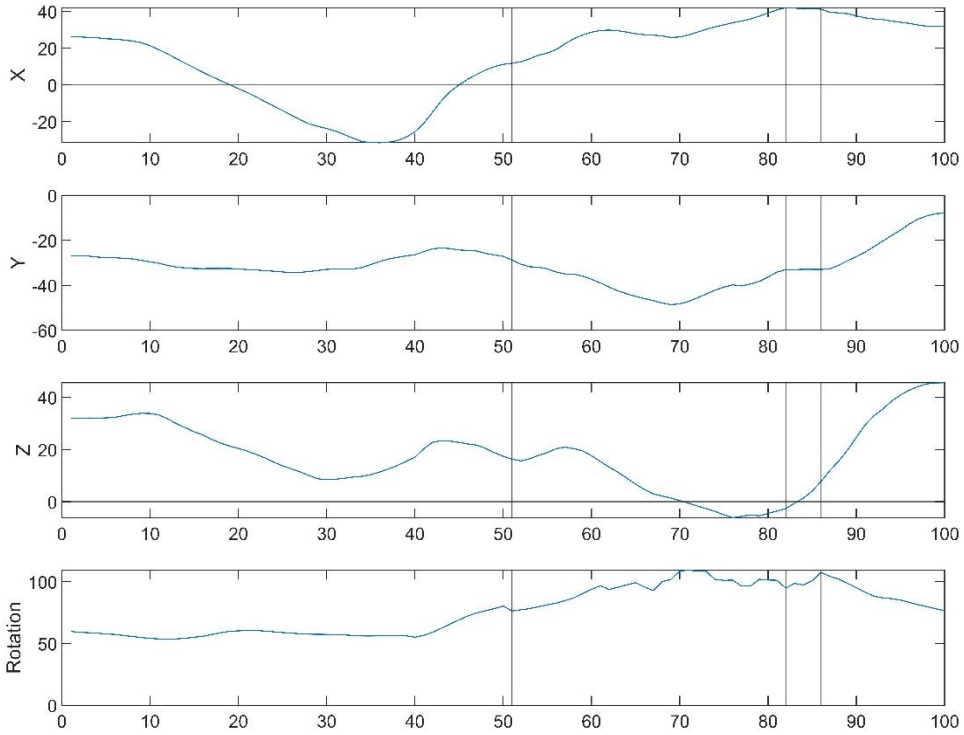

Figure 11. HA Direction Vector and Rotation (°) Line, Same-Side Attack

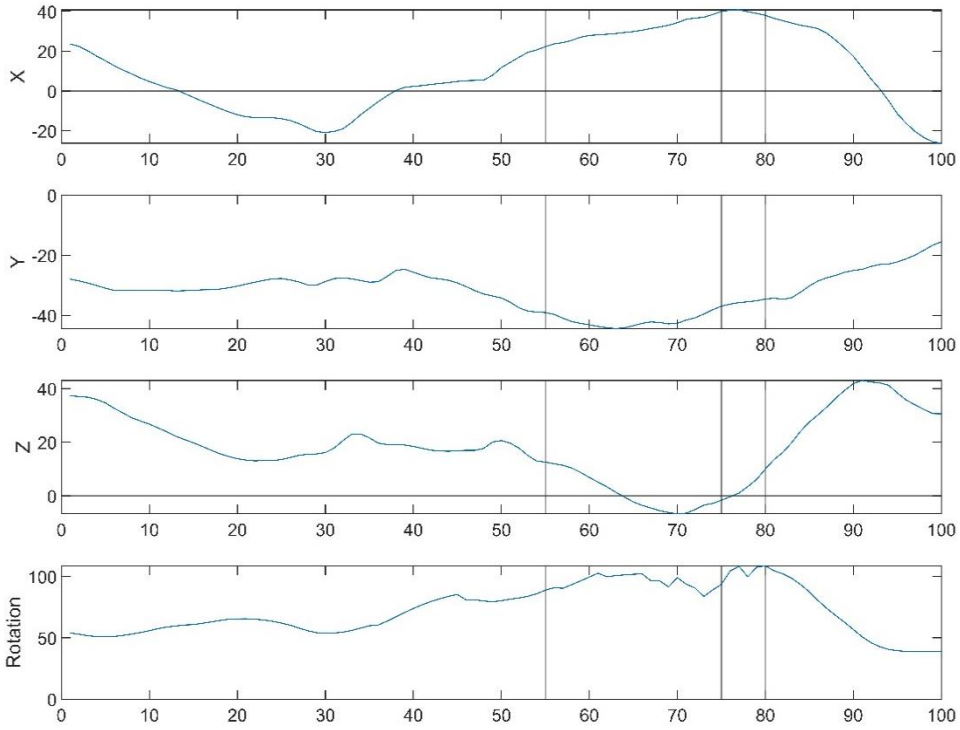

The full attack plots of the Euler angles reveal both similarities and differences in shoulder mechanics across the various volleyball attack types. In general, all attacks show an increase in the plane of elevation and angle of elevation during the arm cocking phase, peaking just before ball contact, and then a decrease during the follow-through phase. However, the degree and pattern of these changes differ between attacks. In the cross-court cross-body attack (Figure 15) and the line cross-body attack (Figure 16), both show increases in the plane and external rotation in the follow-through phase. In contrast, the cross-court same-side attack (Figure 11) and line same-side attack (Figure 15) show decreases in both of these angles.

Figure 12. YXY Euler Sequence (°) Cross-Court, Cross-Body Attack

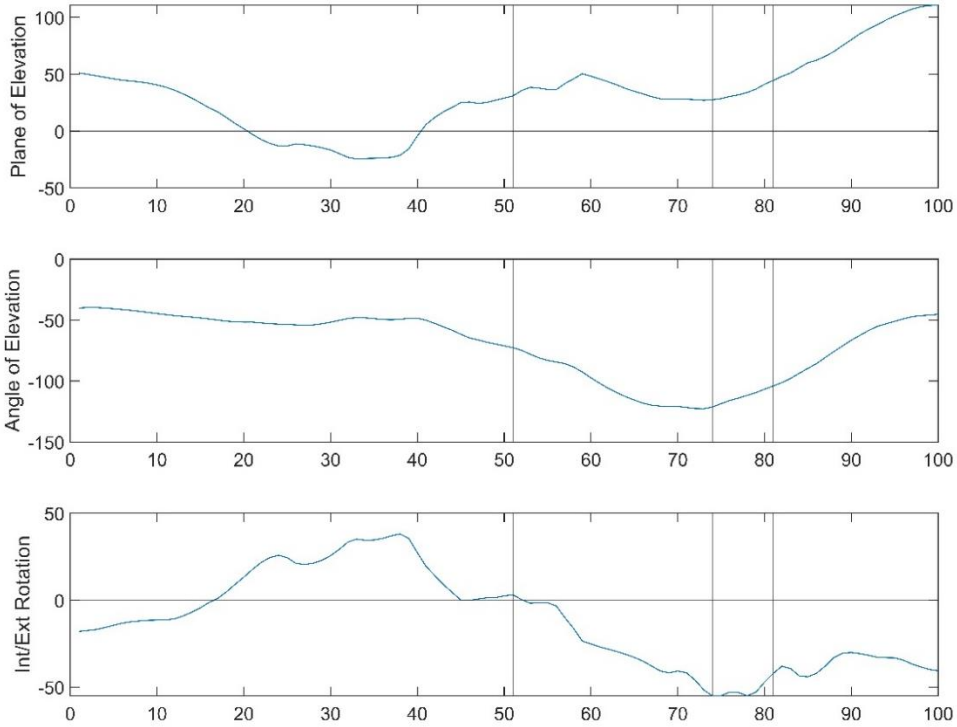

Note: First line indicates the takeoff, second line indicates maximum external rotation of the shoulder, and third line indicates hand contact with the ball for all subsequent plots.

Figure 13. YXY Euler Sequence (°) Cross-Court, Same-Side Attack

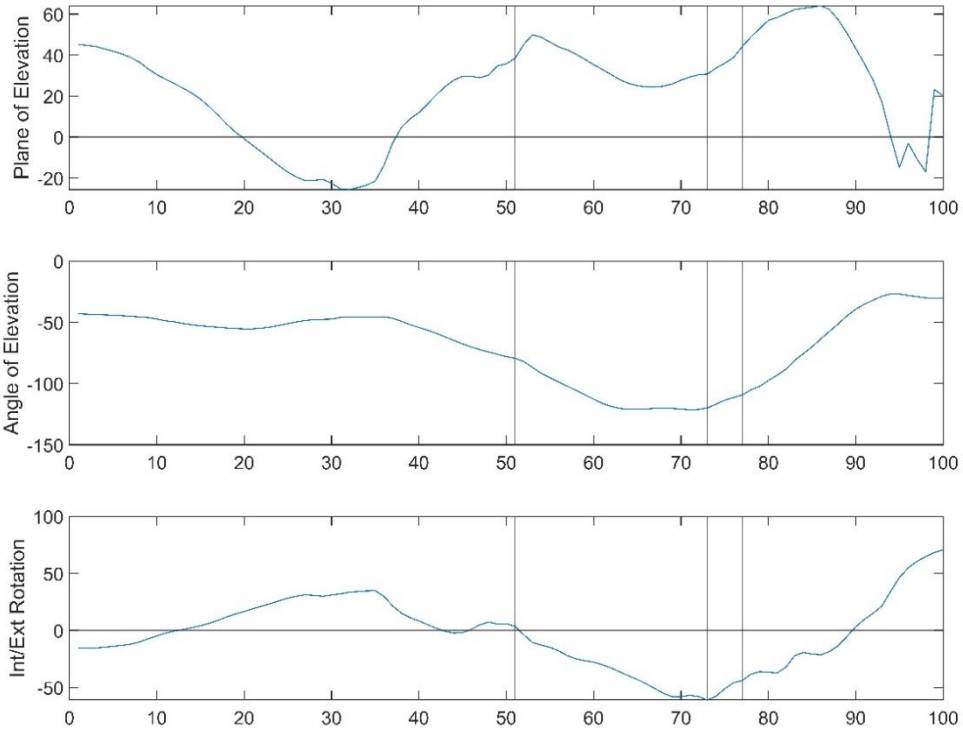

Figure 14. YXY Euler Sequence (°) Line, Cross-Body Attack

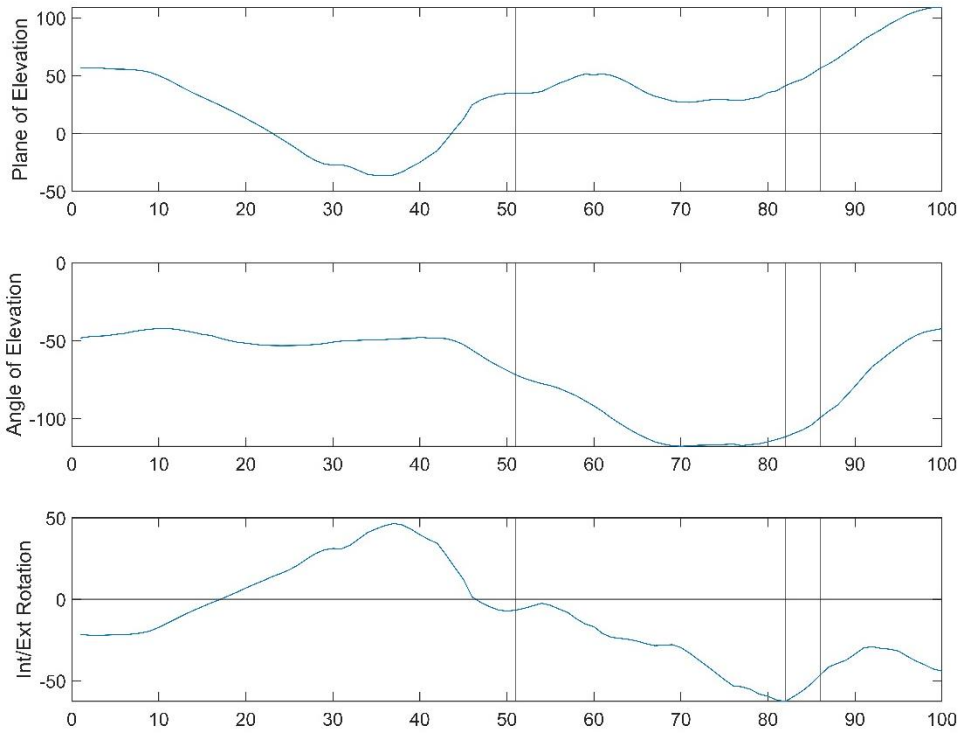

Figure 15. YXY Euler Sequence (°) Line, Same-Side Attack

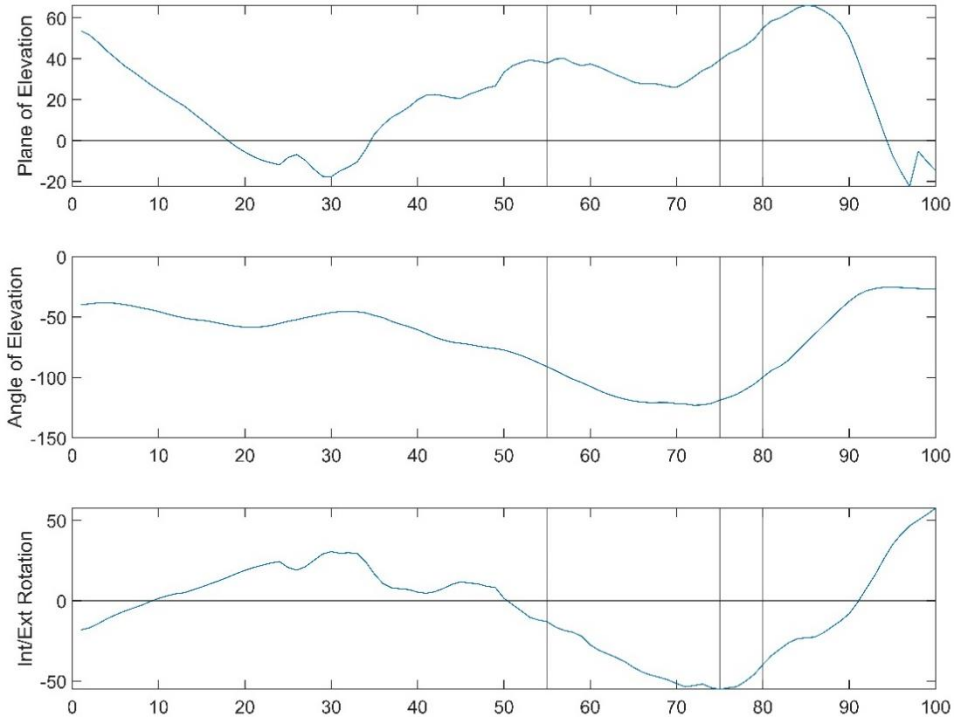

3.2 Approach Phase

Visual analysis showed negligible differences between the different attack styles for all methods of analysis (Figures 16 and 17). An important observation is that at approximately 80% of the approach phase, the angle of rotation about the helical axis suddenly increases. Concurrently, there are noticeable changes in the Y and Z components of the unit vector, suggesting that a specific movement is taking place at this point in the attack. No such pattern exists in the same way when visualizing the Euler angles. This could indicate that the helical axis representation is able to show changes in movement more consistently than the Euler angle method.

Figure 16. Helical Axis Direction Vector and Rotation (°) – Approach

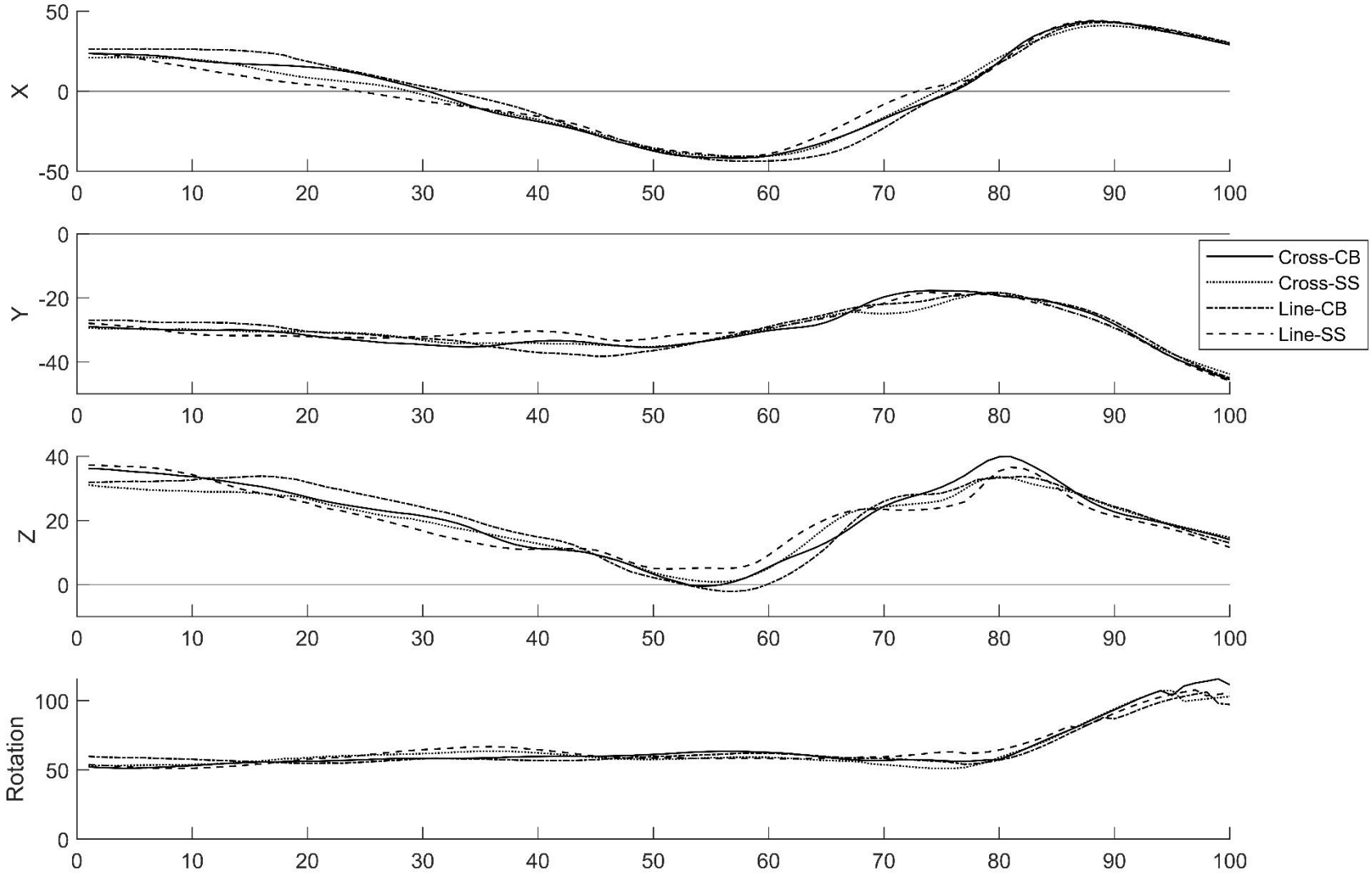

Figure 17. Euler Angles (°) – Approach

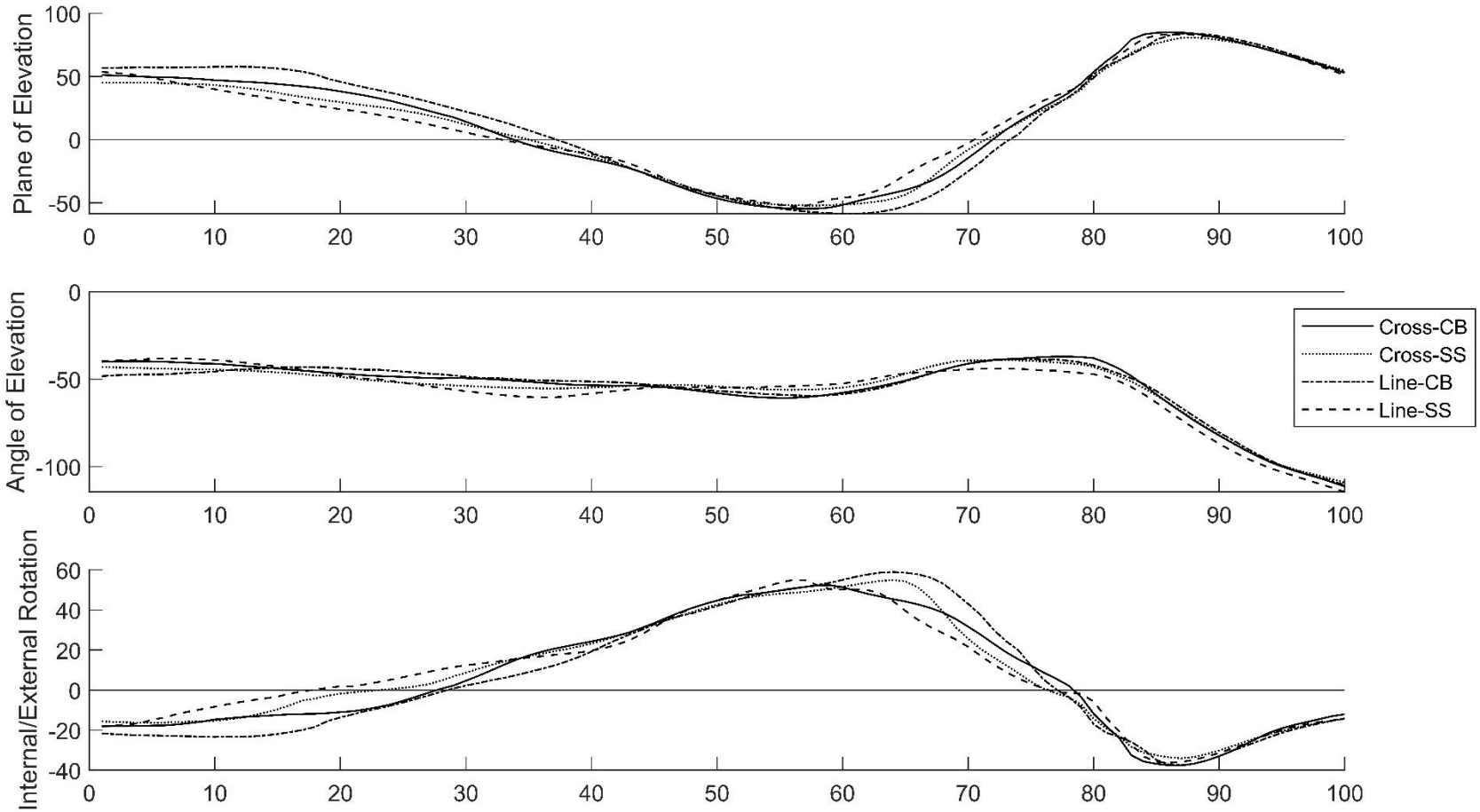

Similarly, the minimum angle, maximum angle, and ROM for the HA method (Table 5) and YXY Euler sequence (Table 6) remained consistent across all conditions for the approach phase. A repeated-measures ANOVA ($p<.05$) was performed on all HA parameters, which indicated no significant differences across conditions. Additionally, ANOVA tests on each Euler representation indicated that there were no significant differences across conditions.

Table 4. Mean (SD) HA Direction Vector and Rotation ROM – Approach

	Condition	Minimum (°)	Maximum (°)	ROM (°)
x	Cross_CB	-50.70 (4.08)	46.57 (4.76)	97.27 (6.57)
	Cross_SS	-51.54 (3.36)	46.95 (4.92)	98.49 (5.65)
	Line_CB	-51.15 (4.14)	47.16 (4.27)	98.32 (7.21)
	Line_SS	-51.70 (3.23)	48.15 (4.23)	99.86 (6.25)
y	Cross_CB	-50.26 (3.78)	-9.76 (6.27)	40.51 (6.19)
	Cross_SS	-49.02 (3.89)	-11.40 (6.77)	37.61 (7.68)
	Line_CB	-49.96 (4.51)	-10.81 (9.71)	39.15 (9.38)
	Line_SS	-49.60 (4.44)	-11.22 (7.39)	38.38 (7.79)
z	Cross_CB	-10.72 (11.74)	53.39 (4.19)	64.11 (11.05)
	Cross_SS	-10.70 (10.20)	53.19 (3.19)	63.90 (8.68)
	Line_CB	-10.77 (11.37)	53.79 (3.37)	64.56 (11.40)
	Line_SS	-10.94 (8.48)	54.41 (2.07)	65.35 (7.92)
Rotation	Cross_CB	32.18 (6.69)	118.74 (13.77)	86.56 (16.46)
	Cross_SS	33.28 (6.86)	116.95 (14.53)	83.67 (16.17)
	Line_CB	31.85 (7.76)	115.92 (15.63)	84.08 (17.29)
	Line_SS	33.89 (8.54)	119.05 (16.10)	85.16 (19.25)

Table 5. Mean (SD) Euler Angles ROM – Approach

	Condition	Minimum (°)	Maximum (°)	ROM (°)
Plane of Elevation	Cross_CB	-65.51 (8.77)	93.32 (9.26)	158.84 (10.09)
	Cross_SS	-67.18 (8.35)	90.35 (11.57)	157.154 (12.60)
	Line_CB	-66.98 (10.05)	92.22 (10.30)	159.20 (15.11)
	Line_SS	-67.42 (9.74)	91.20 (9.62)	158.61 (13.15)
Angle of Elevation	Cross_CB	-111.86 (18.80)	-12.70 (3.37)	99.17 (18.45)
	Cross_SS	-110.20 (21.16)	-13.80 (3.30)	96.40 (21.68)
	Line_CB	-111.26 (18.83)	-12.87 (4.24)	98.39 (19.84)
	Line_SS	-115.44 (18.19)	-12.66 (3.56)	102.78 (19.19)
Int/Ext Rotation	Cross_CB	-52.17 (13.66)	80.95 (15.54)	133.11 (18.31)
	Cross_SS	-52.58 (14.03)	79.25 (12.88)	131.84 (16.28)
	Line_CB	-53.82 (15.52)	82.43 (17.48)	136.25 (24.63)
	Line_SS	-54.67 (14.14)	82.65 (16.17)	137.31 (21.99)

3.3 Arm Cocking Phase

The shoulder angles during the arm cocking phase are shown for each method (Figures 18 and 19). Plots collectively reveal consistent shoulder mechanics during the arm cocking phase across different attack types. Some variation in the angle of rotation about the helical axis has occurred but remains consistent at around 100 degrees.

Figure 18. Helical Axis Direction Vector and Rotation (°) – Arm Cocking

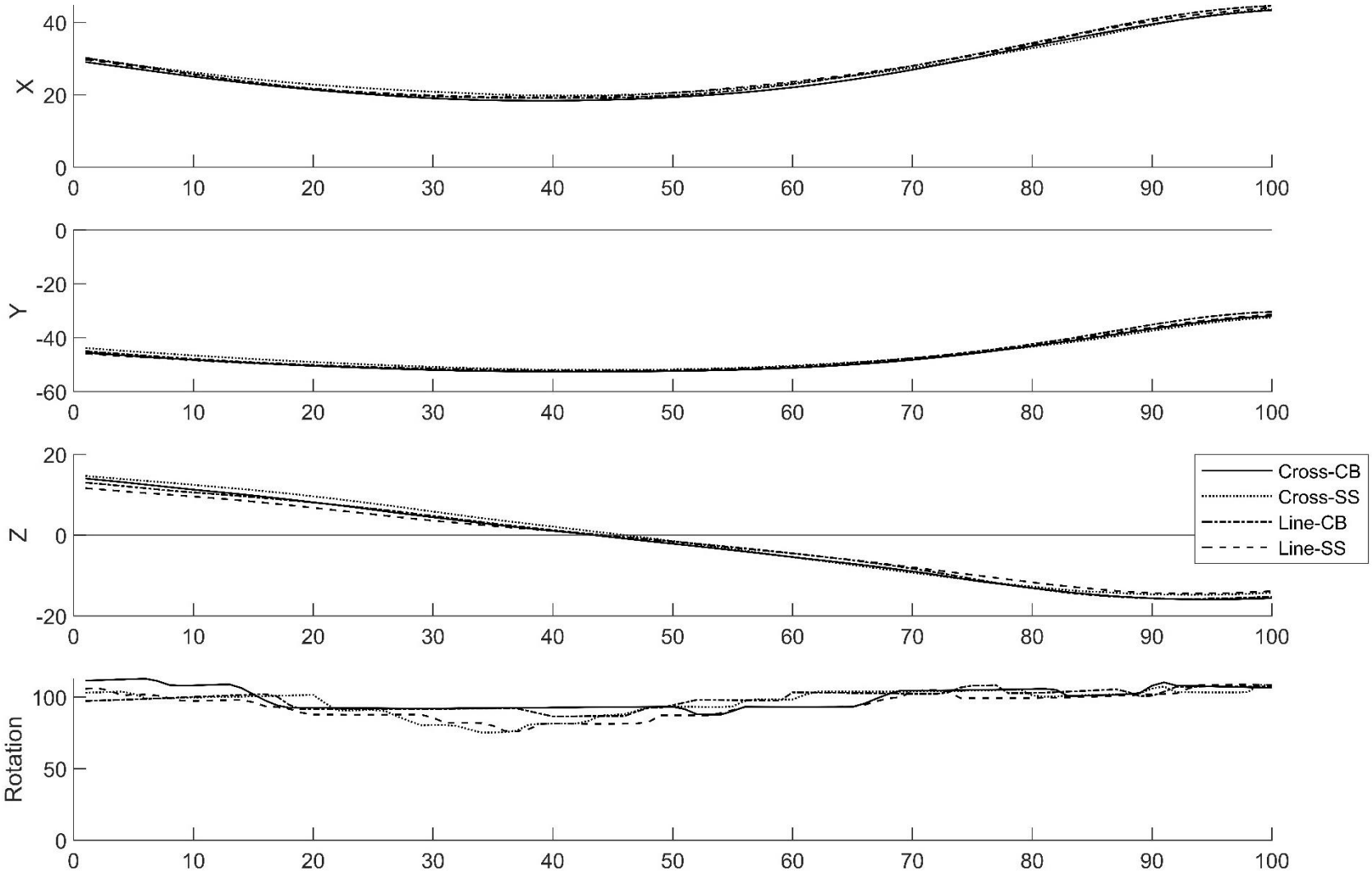

Figure 19. Euler Angles (°) – Arm Cocking

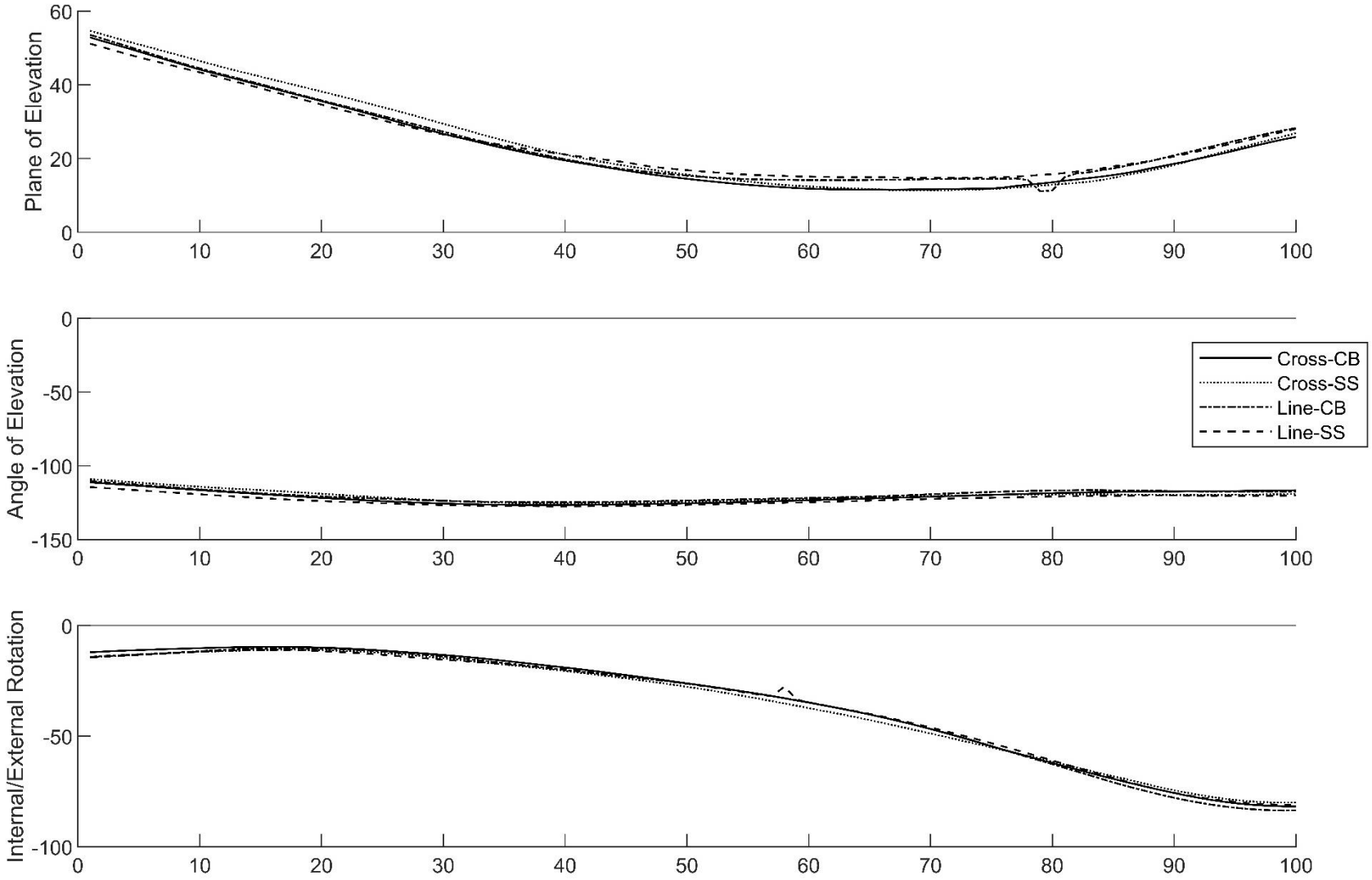

The minimum angle, maximum angle, and ROM for the HA method (Table 7) and YXY Euler sequence (Table 8) remained consistent across all conditions for the arm cocking phase. ANOVA testing indicated no significant differences between conditions for any HA parameter or Euler representation.

Table 6. Mean (SD) HA Direction Vector and Rotation ROM – Arm Cocking

	Condition	Minimum (°)	Maximum (°)	ROM (°)
x	Cross_CB	16.85 (12.49)	43.67 (6.10)	26.82 (11.96)
	Cross_SS	17.75 (12.30)	43.64 (6.26)	25.89 (11.91)
	Line_CB	17.04 (11.74)	44.71 (5.71)	27.67 (12.01)
	Line_SS	17.39 (12.20)	44.10 (6.72)	26.71 (11.41)
y	Cross_CB	-53.16 (4.39)	-31.78 (8.86)	21.37 (8.78)
	Cross_SS	-52.81 (4.04)	-32.16 (8.78)	20.64 (8.58)
	Line_CB	-53.31 (3.40)	-30.35 (9.49)	22.96 (9.63)
	Line_SS	-52.80 (4.34)	-31.37 (9.60)	21.43 (8.84)
z	Cross_CB	-16.86 (5.53)	14.31 (8.42)	31.17 (11.44)
	Cross_SS	-15.73 (4.16)	14.87 (10.79)	30.60 (12.48)
	Line_CB	-16.62 (5.02)	13.19 (8.01)	29.81 (11.06)
	Line_SS	-15.09 (5.43)	11.91 (7.25)	27.00 (10.46)
Rotation	Cross_CB	70.11 (37.92)	130.89 (5.18)	60.78 (40.91)
	Cross_SS	65.14 (35.84)	125.22 (22.38)	60.08 (38.71)
	Line_CB	72.26 (35.60)	129.19 (5.88)	56.93 (39.82)
	Line_SS	69.24 (38.40)	130.89 (5.77)	61.65 (41.62)

Table 7. Mean (SD) Euler Angles ROM – Arm Cocking

	Condition	Minimum (°)	Maximum (°)	ROM (°)
Plane of Elevation	Cross_CB	6.93 (13.87)	53.53 (10.53)	46.60 (15.73)
	Cross_SS	6.67 (12.20)	56.36 (16.06)	49.69 (20.00)
	Line_CB	4.84 (21.34)	54.51 (15.27)	49.67 (26.90)
	Line_SS	10.00 (16.50)	53.23 (12.70)	43.22 (16.66)
Angle of Elevation	Cross_CB	-132.34 (12.35)	-106.19 (17.61)	26.14 (12.37)
	Cross_SS	-132.08 (12.04)	-105.45 (20.64)	26.63 (16.33)
	Line_CB	-130.28 (12.89)	-105.12 (17.50)	25.16 (11.54)
	Line_SS	-132.28 (13.62)	-110.36 (17.29)	21.92 (10.20)
Int/Ext Rotation	Cross_CB	-83.34 (15.96)	-6.83 (16.83)	76.51 (25.00)
	Cross_SS	-81.63 (15.33)	-6.07 (20.98)	75.57 (25.15)
	Line_CB	-84.33 (16.72)	-6.26 (19.32)	78.07 (27.84)
	Line_SS	-81.81 (16.23)	-1.81 (30.40)	79.99 (31.12)

3.4 Arm Acceleration Phase

While a significant difference was only observed in the angle of elevation for Euler angles, a greater visual separation between the curves was evident (Figures 20 and 21). Surprisingly, there were no significant differences between different attack directions for the ROM for any method representation.

Figure 20. Helical Axis Direction Vector and Rotation (°) – Arm Acceleration

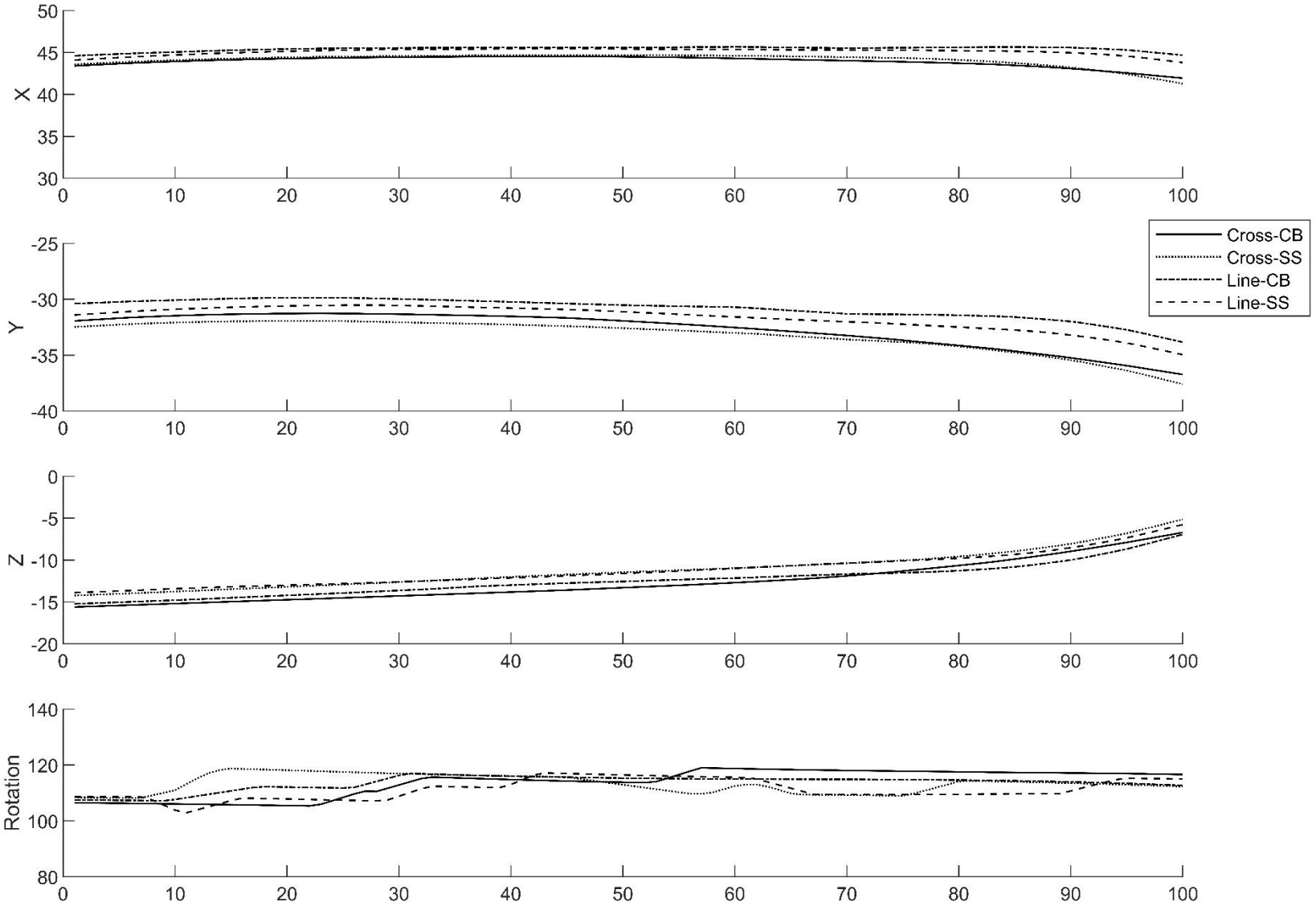

Figure 21. Euler Angles (°) – Arm Acceleration

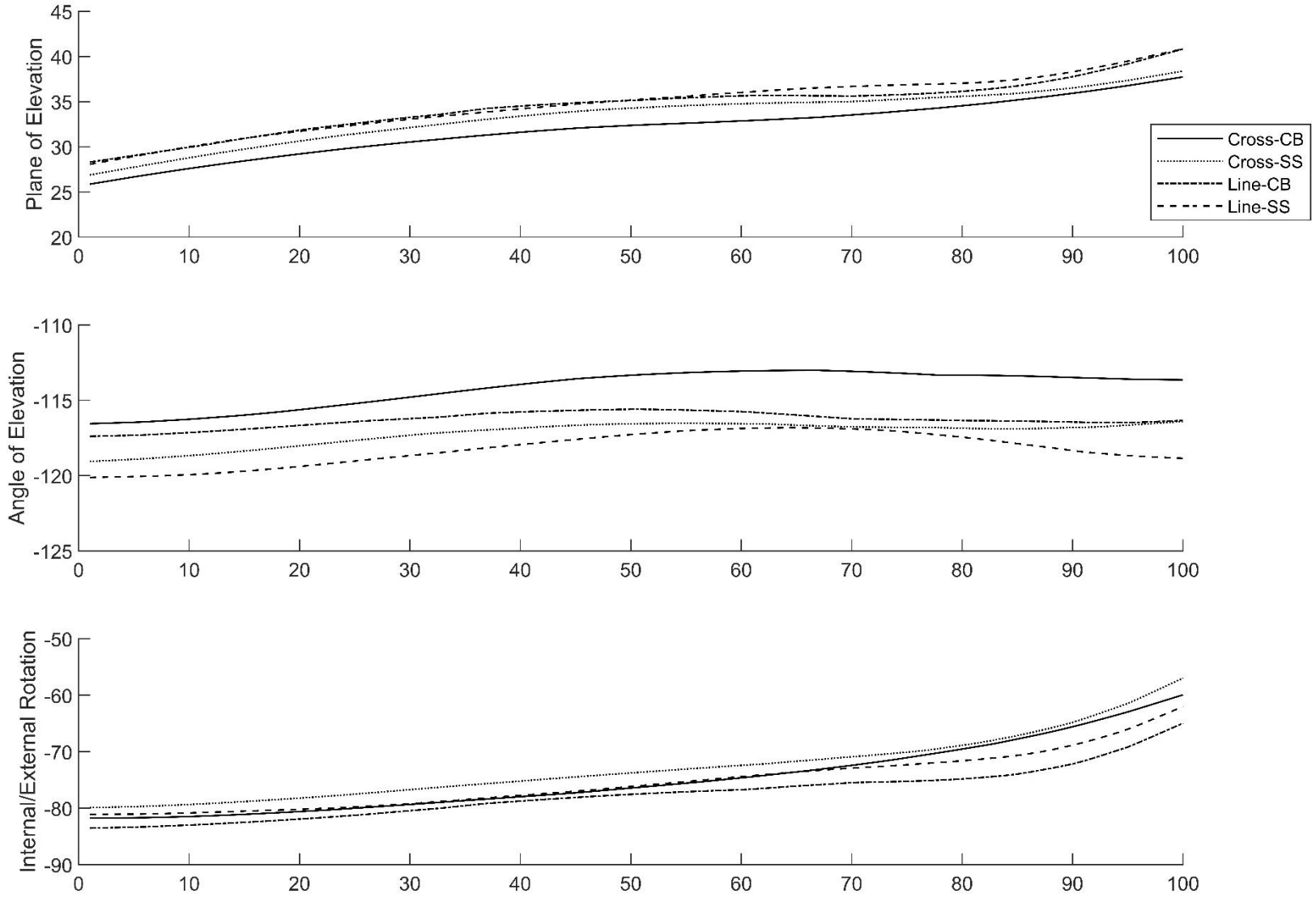

The minimum angle, maximum angle, and ROM for the HA method (Table 9) and YXY Euler sequence (Table 10) were calculated for the arm acceleration phase. ANOVA testing on all HA parameters indicated no significant differences across conditions. Additionally, ANOVA testing was performed on each Euler representation which indicated a significant increase in the minimum angle in the Cross_CB condition compared to Line_SS ($p < .05$).

Table 8. Mean (SD) HA Direction Vector and Rotation ROM – Arm Acceleration

	Condition	Minimum (°)	Maximum (°)	ROM (°)
x	Cross_CB	40.40 (5.41)	45.78 (4.93)	5.38 (4.45)
	Cross_SS	39.45 (7.71)	46.00 (4.45)	6.55 (5.40)
	Line_CB	42.85 (5.03)	46.95 (4.58)	4.10 (3.05)
	Line_SS	42.08 (6.51)	46.55 (5.03)	4.46 (3.43)
y	Cross_CB	-37.86 (6.61)	-29.75 (8.31)	8.11 (8.01)
	Cross_SS	-38.90 (7.27)	-30.34 (7.54)	8.56 (7.08)
	Line_CB	-35.02 (6.84)	-28.25 (8.47)	6.78 (6.90)
	Line_SS	-35.87 (7.52)	-29.37 (8.53)	6.50 (4.89)
z	Cross_CB	-15.85 (5.60)	-6.49 (7.72)	9.36 (8.08)
	Cross_SS	-14.41 (4.56)	-4.69 (5.85)	9.72 (5.16)
	Line_CB	-15.60 (5.16)	-6.57 (5.91)	9.03 (4.78)
	Line_SS	-14.40 (5.11)	-5.50 (5.13)	8.90 (4.82)
Rotation	Cross_CB	99.75 (31.14)	125.37 (7.36)	25.62 (34.93)
	Cross_SS	90.61 (34.79)	127.25 (7.23)	36.64 (39.10)
	Line_CB	101.19 (31.42)	120.90 (21.76)	19.70 (29.52)
	Line_SS	92.33 (36.44)	122.55 (21.83)	30.22 (37.83)

Table 9. Mean (SD) Euler Angles ROM – Arm Acceleration

	Condition	Minimum (°)	Maximum (°)	ROM (°)
Plane of Elevation	Cross_CB	24.19 (12.09)	39.31 (12.03)	15.12 (8.95)
	Cross_SS	26.01 (11.36)	40.08 (9.76)	14.07 (9.07)
	Line_CB	26.80 (11.63)	42.42 (11.63)	15.63 (7.06)
	Line_SS	26.48 (14.86)	42.85 (11.91)	16.37 (9.85)
Angle of Elevation	Cross_CB	-119.72 (7.35)	-109.40 (9.90)	10.32 (7.43)
	Cross_SS	-122.50 (7.02)	-112.43 (11.11)	10.08 (6.71)
	Line_CB	-121.27 (6.64)	-112.16 (10.23)	9.12 (6.60)
	Line_SS	-124.14 (5.90)	-113.79 (6.63)	10.35 (5.29)
Int/Ext Rotation	Cross_CB	-82.64 (15.89)	-59.34 (16.86)	23.31 (22.43)
	Cross_SS	-81.48 (14.66) *	-55.91 (18.43)	25.57 (17.68)
	Line_CB	-85.53 (15.72) *	-63.63 (14.56)	21.90 (14.00)
	Line_SS	-82.73 (15.92)	-60.95 (15.16)	21.78 (10.47)

Note: * indicates significant difference ($p < .05$)

3.5 Follow-Through Phase

The follow-through phase was visualized as having large variations between different follow-through conditions for both methods of analysis (Figures 22 and 23). An important observation is that variations in the helical axis plots consistently occur at around 30% of the phase. However, these variations differ across each Euler angle representation, indicating that the Euler method may not be able to reveal attack patterns as consistently as the helical axis method.

Figure 22. Helical Axis Direction Vector and Rotation (°) – Follow-Through

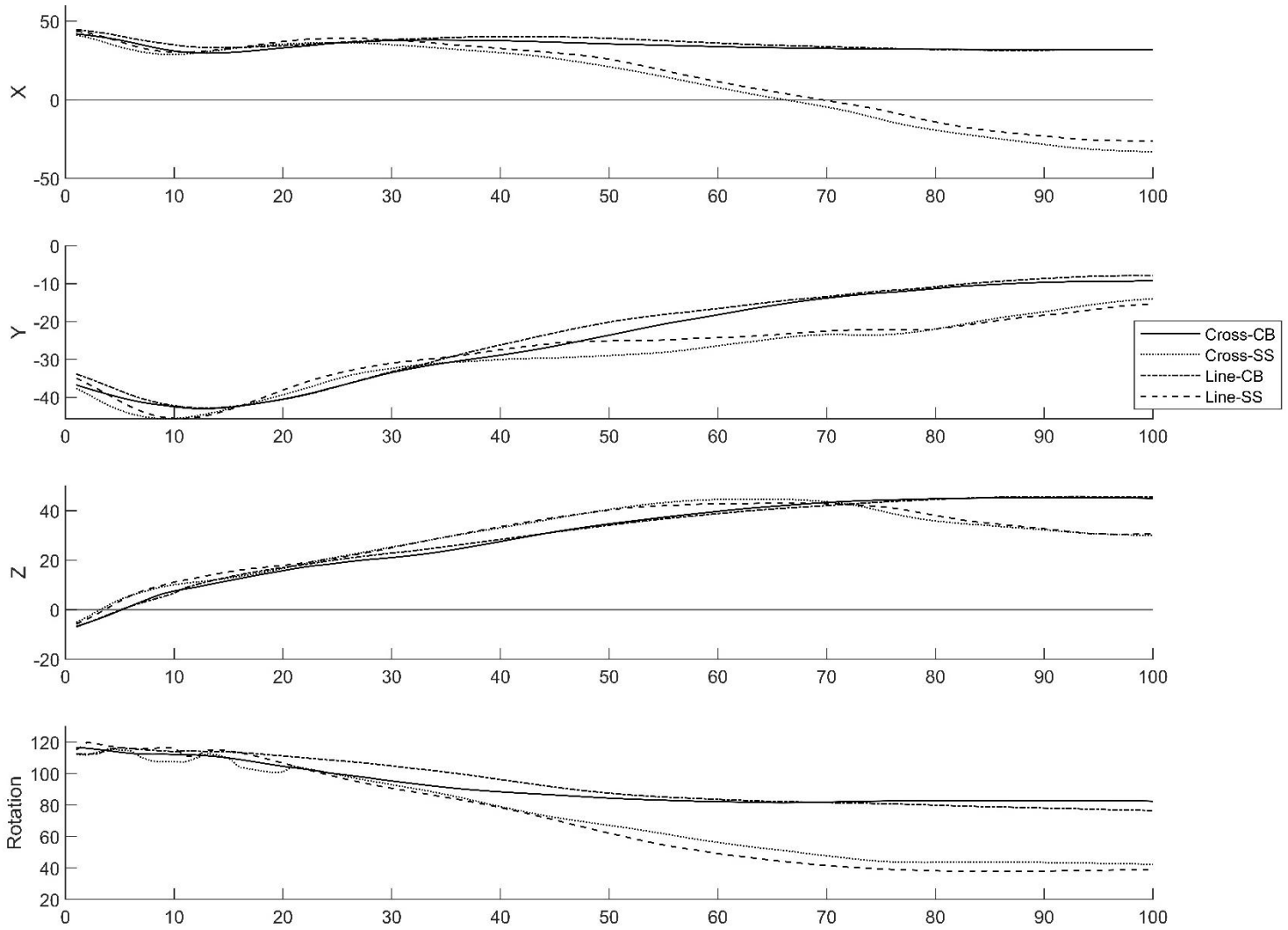

Figure 23. Euler Angles (°) – Follow-through

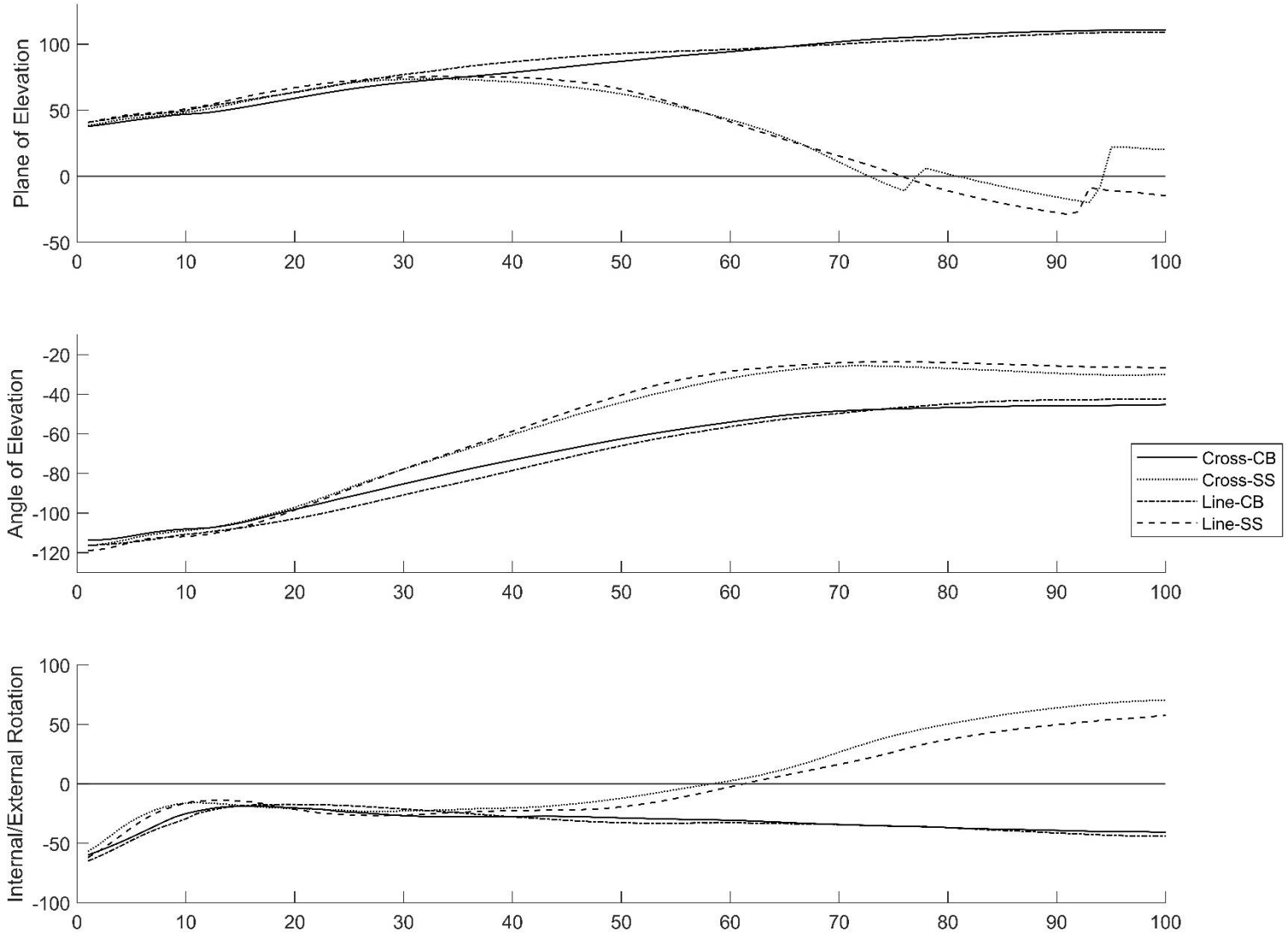

The minimum angle, maximum angle, and ROM for the HA method (Table 11) and YXY Euler sequence (Table 12) were calculated for each condition in the follow-through phase. Significant differences in minimum and ROM in the HA x-direction and angle of rotation were observed across conditions ($p < .001$). Additionally, there were significant differences in the minimum plane of elevation, maximum angle of elevation and axial rotation, as well as ROM across all Euler angles between conditions ($p < .05$ or .001, see Table 12)

Table 10. Mean (SD) HA Direction Vector and Rotation ROM – Follow-through

	Condition	Minimum (°)	Maximum (°)	ROM (°)
x	Cross_CB	22.50 (10.65) [a, b]	46.33 (5.91)	23.83 (8.13) [a, b]
	Cross_SS	-33.40 (19.62) [a, c]	44.97 (5.53)	78.37 (21.28) [a, c]
	Line_CB	26.19 (7.89) [d, c]	47.36 (4.48)	21.16 (7.32) [d, c]
	Line_SS	-29.24 (25.22) [d, b]	45.68 (6.87)	74.92 (27.09) [d, b]
y	Cross_CB	-47.62 (6.11)	-4.94 (6.17)	42.68 (9.52)
	Cross_SS	-49.54 (4.93)	-7.92 (12.30)	41.62 (13.08)
	Line_CB	-45.67 (6.00)	-5.42 (6.06)	40.25 (8.80)
	Line_SS	-47.92 (4.73)	-9.90 (11.36)	38.02 (13.35)
z	Cross_CB	-7.01 (7.08)	46.91 (4.31)	53.91 (7.68)
	Cross_SS	-6.04 (6.08)	50.19 (7.62)	56.22 (9.33)
	Line_CB	-6.94 (6.10)	47.40 (3.74)	54.34 (7.16)
	Line_SS	-6.34 (5.75)	50.34 (6.04)	56.68 (9.04)
Rotation	Cross_CB	70.75 (18.81) [a, b]	118.85 (9.60)	48.10 (20.46) [a, b]
	Cross_SS	35.19 (13.24) [a, c]	120.10 (12.24)	84.91 (15.11) [a, c]
	Line_CB	67.04 (19.33) [d, c]	121.25 (8.82)	54.21 (20.20) [d, c]
	Line_SS	30.11 (12.19) [d, b]	122.49 (7.48)	92.38 (11.31) [d, b]

Note: Paired [a, b, c, d] indicates a significant difference ($p < .001$)

Table 11. Mean (SD) Euler Angles ROM – Follow-Through

	Condition	Minimum (°)	Maximum (°)	ROM (°)
Plane of Elevation	Cross_CB	37.38 (13.37) [a, b]	116.50 (14.77)	79.12 (22.33) [e, f]
	Cross_SS	-47.83 (37.41) [a, c]	114.70 (78.95)	162.54 (99.75) [e, g]
	Line_CB	39.97 (14.08) [d, c]	113.44 (13.46)	73.47 (22.27) [h, g]
	Line_SS	-43.47 (39.88) [d, b]	91.08 (48.85)	134.55 (68.97) [h, f]
Angle of Elevation	Cross_CB	-114.40 (9.49)	-39.53 (10.75) [a, b]	74.87 (14.21) [a, e]
	Cross_SS	-117.48 (11.96)	-16.81 (11.08) [a, c]	100.67 (16.92) [a, f]
	Line_CB	-117.36 (9.55)	-38.20 (10.62) [d, c]	79.16 (11.36) [b, f]
	Line_SS	-119.62 (6.79)	-14.11 (6.41) [d, b]	105.52 (10.43) [b, e]
Int/Ext Rotation	Cross_CB	-64.14 (13.63)	-1.22 (17.57) [a, b]	62.93 (16.89) [a, b]
	Cross_SS	-59.75 (16.10)	73.39 (33.69) [a, c]	133.14 (40.26) [a, c]
	Line_CB	-67.23 (12.56)	-4.24 (14.63) [d, c]	62.99 (15.29) [d, c]
	Line_SS	-63.22 (16.10)	65.09 (38.35) [d, b]	128.31 (38.01) [d, b]

Note: Paired [a, b, c, d] indicates significant difference ($p < .001$), Paired [e, f, g, h indicates] significant difference ($p < .05$)

CHAPTER 4

DISCUSSION

This study completed a comprehensive analysis of shoulder joint kinematics during the volleyball attack, utilizing both the Euler angles and helical axis methods. The primary objective was to determine the kinematic variations across the distinct phases of the volleyball attack: approach, arm cocking, arm acceleration, and follow-through. Furthermore, the study aimed to evaluate the differences in shoulder kinematics between various directional and follow-through conditions within each phase. Finally, to compare the interpretability and accuracy of the Euler angles and helical axis methods to evaluate if the helical axis method is more appropriate for analyzing shoulder movements in volleyball athletes.

4.1 Shoulder Kinematics

The first objective of this study was to calculate shoulder kinematics during each phase of the volleyball attack. Using Vicon motion capture, Visual3d processing, and custom MATLAB programs for calculating Euler Angles and helical axis, this study calculated the kinematics of the shoulder movement through the distinct phases of the attack.

The approach phase in volleyball is characterized by smaller angles with less variability due to its preparatory nature, involving an arm swing below the head level. This phase acts as a setup for the jump, where athletes often use a consistent approach technique across various attack types to maintain uniformity and maximize effectiveness (Baena et al., 2021). This consistent approach helps players achieve the necessary momentum and positioning for the subsequent phases of the attack. The angle of rotation about the helical axis averaged to around

64° with minimums at about 30° and maximums almost 120°. The mean angle about the helical axis increased in the arm cocking phase to around 100° and increased further to 113° during the arm acceleration phase. During the follow-through phase, the helical axis angle of rotation decreased. This will be explored in the next section, as there were significant differences in the HA in the follow-through phase between conditions.

The Euler angles offered a more straightforward representation of the shoulder's anatomical movements. During the approach phase, the arm was internally rotated about 6°, indicated by the positive axial rotation value. This rotation does increase as the arm swing progresses, with rotations reaching about 80° and dipping at -52°. Also, during the approach phase, the arm reaches an angle of elevation of about -55° throughout a 15° plane. This indicates that the arm is abducted with some forward flexion and backward extension as the player performs the approach (Barrett et al., 2024).

During the arm cocking phase, the shoulder elevates to about -120° and prepares to enter the acceleration phase when it reaches maximum external rotation at about -84°. During the arm acceleration phase, the shoulder remains in a plane of elevation between about 24° and 42°, with the average at about 33°. This indicates that the shoulder is abducted with some flexion as the hand contacts the ball. The follow-through phase had a wide variability in both helical axis and Euler angle representations, as two different follow-through strategies were used.

The quantified shoulder kinematics during each phase of the volleyball attack indicate that consistent patterns and variations in shoulder movements occur in all phases of the volleyball attack. Building on these insights, exploring the differences between each attack condition could further indicate which mechanics influence the kinematics at the shoulder.

4.2 Differences Across Conditions

The second goal of this study was to analyze the statistical differences in shoulder kinematics across different attack directions (cross-court and line) and follow-through strategies (cross-body and same-side). Significance testing revealed some differences in shoulder kinematics across conditions, particularly in the follow-through phase.

No significant effects were found in the approach or arm cocking phases for either the helical axis or Euler representations of mean, minimum, or maximum angles. This is likely because participants were healthy and do not change their approach or arm cocking depending on the direction of the attack or follow-through. Furthermore, the additional benefits to the traditional approach, including greater initial position flexibility, more efficient horizontal-to-vertical impulse transfer, better in-air positioning, and a wider range of attack placements, could reinforce its popularity (Zahálka et al., 2017).

In the arm acceleration phase, there was a significant increase in external rotation in the Cross_SS condition compared to the Line_CB condition only. Because both direction and follow-through were varied and it was the only significant differences based on direction in the arm acceleration phase, it is unclear which condition played a role in the difference. Nonetheless, the difference was significant according to a repeated-measures ANOVA test ($p<.05$). Interpreting this result, when participants were asked to hit cross-court finishing on the same side, their shoulder was more internally rotated during the acceleration phase than when hitting a line attack and following through cross-body, which is not consistent with previous findings suggesting that increased internal rotation is associated with line attacks (Brown et al., 2014).

The follow-through phase saw the most significant differences between conditions. The HA rotational angle was significantly smaller in both same-side follow-through conditions, with an average angle of about 70° compared to the cross-body counterparts, both with angles around

90°. The plane of elevation saw large differences as well, with angles of about 38° for the same-side conditions and 85° for the cross-body conditions. This indicates that the cross-body follow-through is almost pure abduction, while the same side leans more towards extension (Reeser et al., 2010). The angle of elevation and internal/external rotation follow the opposite pattern, with larger angles under the same-side conditions.

4.3 Limitations and Future Work

While this study provides valuable insights into shoulder kinematics during the volleyball attack, several limitations should be noted. Firstly, the sample size was small, which may limit the generalizability of the findings. Future research should include a larger and more diverse sample to validate these results. Additionally, the motion capture system, while advanced, may still have inherent inaccuracies in capturing rapid movements. Further studies could benefit from incorporating complementary technologies, such as high-speed cameras or wearable inertial measurement units, to enhance data accuracy.

All angle calculations were performed in MATLAB using custom programs, which can lead to inconsistencies with other motion processing software, such as Visual3d. Moreover, this study focused solely on shoulder kinematics; future work could expand to analyze the interaction of shoulder movements with other body segments. Additionally, there did appear to be large variations in the helical axis orientation between subjects, which could influence the significance of the results. Future work would look at the average helical axis to determine differences between participants. Lastly, other methods of measuring joint kinematics, such as the Grood and Suntay joint coordinate system, should be compared to determine the most appropriate technique (Grood & Suntay, 1983).

4.4 Conclusion

When comparing the interpretability of the Euler angle and helical axis methods, both offer unique advantages. Euler angles provide a straightforward representation of shoulder anatomical movements, making it easier to understand and visualize the joint's rotations in terms of the three primary movements. However, the helical axis method captures the complex, three-dimensional nature of shoulder movement more comprehensively, offering detailed insights into the rotational axis and angle of rotation. While Euler angles are useful for simpler, more intuitive analyses, the helical axis method could be more accurate to describing the 3-D motion of the shoulder, while additionally revealing more consistent patterns that the Euler angle method does not show.

This study quantified shoulder kinematics during each phase of the volleyball attack using Euler angle and helical axis analysis of motion capture data. Key findings include consistency in the approach phase, the quantification of the maximum external rotation during the arm cocking phase, and shoulder elevation during the arm acceleration phase. The follow-through phase showed varied kinematics, reflecting the various directional and follow-through conditions. These insights are important to understand the kinematics of the volleyball attack, which has implications for future studies aimed at enhancing training and injury prevention strategies.

APPENDICES

Appendix A. Custom MATLAB Function to Calculate YXY Euler Sequence

```
function euler_angles = computeEulerAnglesYXY(rotation_matrices)
    % Computes the Euler angles using the YXY sequence recommendeded by the
    % ISB for measuring shoulder kinematics.
    %
    % Input:
    %   rotation_matrices - 3x3 matrix containing 100 rotation matrices
    %
    % Output:
    %   euler_angles - 3x100 matrix containing the Euler angles (thetaX, thetaY0,
thetaY1)
    %                  for each rotation matrix in the sequence YXY

    % Initialize the output matrix for Euler angles
    euler_angles = zeros(3, size(rotation_matrices,3));

    for i = 1:size(rotation_matrices,3)

        R = rotation_matrices(:, :, i);


        if R(3,3) < 1

            if R(3,3) > -1

                thetaX = -acos(R(3,3));

                thetaY0 = atan(R(1,3)/-R(2,3)) + (pi/2);

                thetaY1 = atan(R(3,1)/R(3,2)) - (pi/2);

                % Need to adjust the angle of Y0
                if -R(2,3) > 0
                    thetaY0 = thetaY0;
                elseif -R(2,3) < 0 && R(1,3) >= 0
                    thetaY0 = thetaY0 + pi;
                elseif -R(2,3) < 0 && R(1,3) < 0
                    thetaY0 = thetaY0 - pi;
                elseif -R(2,3) == 0 && R(1,3) > 0
                    thetaY0 = pi/2;
                elseif -R(2,3) == 0 && R(1,3) < 0
                    thetaY0 = -pi/2;
                else
                    thetaY0 = 0;
                end

                 % Need to adjust the angle of Y1
                if R(3,2) > 0
                    thetaY1 = thetaY1;
                elseif R(3,2) < 0
                    thetaY1 = thetaY1 + pi;
                elseif R(3,2) == 0 && R(3,1) > 0
```

```
                thetaY1 = pi/2;
            elseif R(3,2) == 0 && R(3,1) < 0
                thetaY1 = -pi/2;
            else
                thetaY1 = 0;
            end

        else % R(3,3) = -1

            thetaX = -pi;
            thetaY0 = -atan2(-R(1,2),R(1,1))+(pi/2);
            thetaY1 = -pi/2;

        end

    else % R(3,3) = 1

        thetaX = 0;
        thetaY0 = atan2(-R(1,2),R(1,1))+(pi/2);
        thetaY1 = pi/2;

    end

     % Store the computed angles
    euler_angles(:, i) = [thetaY0; thetaX; thetaY1];

end

end
```

Appendix B. Custom MATLAB Function to Calculate Helical Axis

```
function [FHA_ang, FHA_n] = calculateFHA(RotM)
% Calculates the Finite Helical Axis angle of rotation, axis unit vector
% based on the method proposed by Spoor and Veldpaus, 1980.
%
% Input:
    % Rotation Matrix 3x3xn
%
% Outputs:
    % FHA_ang: angle of rotation
    % FHA_n: unit vector

    % Preallocate variables
    FHA_ang = nan(size(RotM,3),1);
    FHA_n = nan(size(RotM,3),3);

    % FHA Calculation
    for i = 1:size(RotM,3)
        diff_vector = [RotM(3,2,i) - RotM(2,3,i);
                       RotM(1,3,i) - RotM(3,1,i);
                       RotM(2,1,i) - RotM(1,2,i)];

        FHA_sinang = sqrt(sum(diff_vector.^2)) / 2;
        FHA_cosang = (RotM(1,1,i) + RotM(2,2,i) + RotM(3,3,i) - 1) / 2;

        if FHA_sinang <= sqrt(2) / 2
            FHA_ang(i) = asin(FHA_sinang);
        else
            FHA_ang(i) = acos(FHA_cosang);
        end

        FHA_n(i,:) = (1 / (2 * sin(FHA_ang(i)))) * ...
                     [RotM(3,2,i) - RotM(2,3,i),
                      RotM(1,3,i) - RotM(3,1,i),
                      RotM(2,1,i) - RotM(1,2,i)];
    end

    % Convert to Degrees
    FHA_ang = rad2deg(FHA_ang);
    FHA_n = rad2deg(FHA_n);

end
```

REFERENCES

Baena-Raya A, Soriano-Maldonado A, Rodríguez-Pérez MA, García-de-Alcaraz A, Ortega-Becerra M, Jiménez-Reyes P, et al. (2021) The force-velocity profile as determinant of spike and serve ball speed in top-level male volleyball players. *PLoS ONE 16*(4).

Bakhsh, W., & Nicandri, G. (2018). Anatomy and physical examination of the shoulder. *Sports Medicine and Arthroscopy Review*, *26*(3).

Barrett, K. B., Parrish, K., Bennett, H. J. (2024) Rotation sequences for the calculation of shoulder kinematics of the volleyball attack.

Biga, L. M., Bronson, S., Dawson, S., Harwell, A., Hopkins, R., Kaufmann, J., LeMaster, M., Matern, P., Morrison-Graham, K., Oja, K., Quick, D., & Runyeon, J. (2019, September 26). *9.6 anatomy of selected synovial joints*. Anatomy Physiology.

Brown, J. R., Alsarraf, B. J., Waller, M., Eisenman, P., & Hicks-Little, C. A. (2014). Rotational angles and velocities during down the line and diagonal across court volleyball spikes. International Journal of Kinesiology and Sports Science, 2(2), 1–8.

Cattrysse E, Baeyens J, Roy P, Van W, De V, Roosens T, Clarys J. (2007). Intra-articular kinematics of the upper limb joints: a six degrees of freedom study of coupled motions Intra-articular kinematics of the upper limb joints: a six degrees of freedom study of coupled motions. *Ergonomics. 48*:11–14(Oct 2014), 1657–1671.

Challoumas, D., & Artemiou, A. (2018). Predictors of Attack Performance in High-Level Male Volleyball Players. *International Journal of Sports Physiology and Performance*, *13*(9), 1230-1236.

Chandran, A., Morris, S. N., Lempke, L. B., Boltz, A. J., Robison, H. J., & Collins, C. L. (2021). Epidemiology of Injuries in National Collegiate Athletic Association Women's Volleyball: 2014-2015 Through 2018-2019. *Journal of Athletic Training*, *56*(7), 666–673.

Chao, E. Y. S. (1980). Justification for triaxial goniometer for the measurement of joint rotation. *Journal of Biomechanics, 13*(12), 989-993, 995-1006.

Chu, Y., Fleisig, G. S., Simpson, K. J., & Andrews, J. R. (2009). Biomechanical comparison between elite female and male baseball pitchers. *Journal of Applied Biomechanics*, *25*(1), 22–31.

Cripton P. A., Sati M., Orr T. E., Bourquin Y., Dumas G. A., Nolte L. P. (2001). Animation of in vitro biomechanical tests. *Journal of Biomechanics. 34*(8):1091–1096.

Delgado, P., Alekhya, S., Majidirad, A., Hakansson, N.A., Desai, J., Yihun, Y. (2010) Shoulder Kinematics Assessment towards Exoskeleton Development. *Applied Sciences, 10*(18): 6336.

Eberly, D. (1999). Euler Angle Formulas. *Geometric Tools*. https://www.geometrictools.com/Documentation/EulerAngles.pdf

Elliott, B., Fleisig, G., Nicholls, R., & Escamilia, R. (2003). Technique effects on upper limb loading in the tennis serve. J*ournal of Science and Medicine in Sport, 6*(1), 76–87.

Fédération Internationale de Volleyball. (n.d.). The FIVB. The FIVB: Structure. https://www.fivb.com/en/thefivb/structure

Goldfarb, N., Lewis, A., Tacescu, A., Fischer, G. S. (2021). Open source Vicon Toolkit for motion capture and Gait Analysis. *Computer Methods and Programs in Biomedicine, 212*, 106414

Grip H, Sundelin G, Gerdle B, Stefan Karlsson J. (2008). Cervical helical axis characteristics and its center of rotation during active head and upper arm movements-comparisons of whiplash-associated disorders, non-specific neck pain and asymptomatic individuals. *Journal of Biomechanics, 41*(13):2799–2805

Grood, E. S., & Suntay, W. J. (1983). A joint coordinate system for the clinical description of three-dimensional motions: application to the knee. Journal of biomechanical engineering, 105(2)

Haneline, M. T., Cooperstein, R., Young, M. D., & Ross, J. (2008). Determining spinal level using the inferior angle of the scapula as a reference landmark: A retrospective analysis of 50 radiographs. *The Journal of the Canadian Chiropractic Association, 52*(1), 24–29.

Karduna, A. R., McClure, P. W., Michener, L. A. (2000). Scapular kinematics: effects of altering the Euler angle sequence of rotations. *Journal of Biomechanics, 33*(9), 1063-1068.

Kritzer, T. D., Lang, C. J., Holmes, M. W. R., & Cudlip, A. C. (2024). Sex differences in strength at the shoulder: a systematic review. *PeerJ*, *12*, e16968.

Kugler, A., Krüger-Franke, M., Reininger, S., Trouillier, H. H., & Rosemeyer, B. (1996). Muscular imbalance and shoulder pain in volleyball attackers. *British Journal of Sports Medicine, 30*(3), 256–259.

Leagues. (n.d.). Tidewater Volleyball Association. Retrieved July 15, 2024, from https://playtva.org/club/leagues.

Ludewig, P. M., Reynolds, J. F. (2009). The association of scapular kinematics and glenohumeral joint pathologies. Journal of Orthopaedic & Sports Physical Therapy, 39(2), 90-104. https://doi.org/10.2519/jospt.2009.39.2.90

Phadke, V., Braman, J. P., LaPrade, R. F., Ludewig, P. M. (2011). Comparison of glenohumeral motion using different rotation sequences. *Journal of Biomechanics, 44*(4), 700-705.

Rab, G., Petuskey, K., & Bagley, A. (2002). A method for determination of upper extremity kinematics. *Gait & Posture, 15*(2), 113–119.

Reeser, J. C., Fleisig, G. S., Bolt, B., Ruan, M. (2010). Upper limb biomechanics during the volleyball serve and spike. *Sports Health, 2*(5), 368-374.

Sheehan, F. T. (2010). The instantaneous helical axis of the subtalar and talocrural joints: a non-invasive in vivo dynamic study. Journal of Foot and Ankle Research, 3(13). https://doi.org/10.1186/1757-1146-3-13

Spoor, C. W., & Veldpaus, F. E. (1980). Rigid body motion calculated from spatial co-ordinates of markers. *Journal of Biomechanics*, *13*(4), 391–393.

Woltring, H. J. (1991). Representation and calculation of 3-D movement. *Human Movement Sciences, 10*, 603-616.

Wu, G., van der Helm, F. C. T., (DirkJan) Veeger, H. E. J., Makhsous, M., Van Roy, P., Anglin, C., Nagels, J., Karduna, A. R., McQuade, K., Wang, X., Werner, F. W., & Buchholz, B. (2005). ISB recommendation on definitions of joint coordinate systems of various joints 75 for the reporting of human joint motion—Part II: Shoulder, elbow, wrist and hand. *Journal of Biomechanics, 38*(5), 981–992.

Zahálka, F., Malý, T., Malá, L., Ejem, M., & Zawartka, M. (2017). Kinematic Analysis of Volleyball Attack in the Net Center with Various Types of Take-Off. *Journal of Human Kinetics*, *58*, 261–271.

VITA

Victoria Jolliff, a native of Morgantown, WV, graduated from University High School in 2018 as a member of the National Honor Society and an Advanced Placement Scholar. She went on to attend West Virginia University, where she received her Bachelor of Science in Biomedical Engineering with a minor in Medical Humanities and Health Studies in 2022. During her time at WVU, she was a member of the Honors College and actively participated in student organizations such as Remote Area Medical and the Society of Women Engineers. Her senior capstone project focused on the mechanical fatigue of an auditory prosthetic device.

Continuing her education at Old Dominion University, Victoria engaged in several student organizations, including the American Society of Biomechanics and the Graduate Student Government Association. As a Graduate Research Assistant under Dr. Stacie I. Ringleb, she contributed to a human factors SBIR project with VR Rehab, Inc. (VRR), developing the SAIPAN (Single Amphibious Integrated Precision Augmented Reality Navigation) system. This project involved simulation testing with university students and presenting findings at the MODSIM World and American Society of Biomechanics conferences in 2024. Additionally, she conducted operational use testing, providing feedback to the VRR team to enhance the software based on human factors principles. Victoria's academic and research experiences have equipped her with a strong foundation in biomechanics and human factors, preparing her for future contributions to the field.